Increasing the affinity between a targeted axonal import (TAxI) peptide and its target receptor hLamR

Po-Chun Wang

A thesis
submitted in partial fulfillment of the
requirements for the degree of

Master of Bioengineering

University of Washington

2021

Committee:
Drew L. Sellers
James J. Lai

Program Authorized to Offer Degree:
Bioengineering

University of Washington

Abstract

Increasing the affinity between a targeted axonal import (TAxI) peptide and its target receptor hLamR

Po-Chun Wang

Chair of the Supervisory Committee:
Drew L. Sellers
Department of Biochemistry

An efficient delivery approach for trafficking therapeutics into central nervous system (CNS) is a critical unmet need. Previously, we identified a target axonal import (TAxI) peptide that delivers protein cargo into the central nervous system (CNS), especially the spinal cord and hindbrain, via retrograde axonal transport mechanism after peripheral administration. Mass spectrometry analysis of a TAxI peptide pull-down assay suggested that human laminin receptor (hLamR) is the potential binding target for TAxI peptide. However, the evidence of interaction between TAxI and hLamR is still lacking. Moreover, the binding affinity of TAxI peptide has yet to be optimized. Here, we report that TAxI binds to cells that express hLamR on the cell membrane. Moreover, a fluorescence activated cell sort (FACS) correlation study proved that TAxI binds hLamR directly. Through sequence modification and multivalent polymerization, the affinity of TAxI-based peptides and co-polymer formulations was optimized and demonstrated increased hLamR binding-affinity. In particular, the binding between Poly-TAxI and hLamR was significantly enhanced due to avidity effects in high hLamR expressing cells. Chondroitin sulfate is shown to be an allosteric modulator for facilitating association between TAxI and hLamR. Interestingly, TAxI showed robust binding to multiple cancer cells with relative abundant membrane level of hLamR, compared to the non-cancer cell. In addition, we also present the development and optimization of a workflow to express and purify recombinant hLamR protein expressed in eukaryotic cells. TAxI-based peptide and co-polymer formulations are able to target high hLamR expressing cells, and thus demonstrates the protential potential to target the delivery of promising therapeutics into the CNS.

Table of Contents

Literature Review

Common Neurodegenerative Diseases

Alzheimer's disease (AD) is a neurodegenerative disease caused by the formation of plaques and neurofibrillary tangles composed of β-amyloid and tau proteins, respectively (Taylor et al., 2002; Buckner et al., 2005). It's one of the most frequent observed form of dementia, and the risk is positively associated with age. No new drug has been approved by FDA for AD since 2003, the only medications for AD on the market are acetylcholinesterase inhibitors (AChEIs) such as donepezil, galantamine, rivastigmine and the N-Methyl-D-aspartic (NMDA) acid antagonist, memantine (Atri, 2019). AChEIs aim to reduce the breakdown of acetylcholine amounts in the brain of the patients with AD by suppressing the responsible enzyme acetylcholinesterase in the synaptic cleft (Yiannopoulou and Papageorgiou, 2013). Hence, the central cholinergic neurotransmission is enhanced by AChEIs and tended to mitigate decline in cognition (Howard et al., 2015). On the other hand, memantine is a noncompetitive low-affinity NMDA-receptor open-channel blocker and affects glutamatergic transmission (Yiannopoulou and Papageorgiou, 2013). FDA approved the use of memantine for moderate and severe AD either as monotherapy or in combination with an AChEI (Scheltens et al., 2016).

Parkinson's disease (PD) is characterized by the privation of dopaminergic neurons in the substantia nigra. The disease progress is associated with accumulation of ubiquitinated α-synuclein in the dopaminergic neurons. Parkinsonism consists of tremor, stiffness, bradykinesia, akinesia, cognitive decline, depression and anxiety (Armstrong and Okun, 2020; Weintraub et al., 2008). As there is currently no exact cure for PD, and there are no known agents to slow down PD progression; the current treatments are used to ameliorate the symptoms of PD. There are a variety of treatments available, such as dopamine precursor, levodopa, catechol-O-methyl transferase (COMT) inhibitors, dopamine agonists, anti-cholinergics, amantadine and monoamine oxidase (MAO) inhibitors (Weintraub et al., 2008).

Barriers to Central Nervous System (CNS) Delivery

Delivering drug into the brain is one of the most critical hurdles to CNS therapy. Reports have estimated that almost 100% of small molecule drugs and biologics are excluded from the CNS due to delivery barriers. Three major barriers for CNS delivery are the blood–brain barrier (BBB), the blood cerebrospinal fluid (CSF) barrier, and dilution effects due to the systemic distribution of drug.(Pardridge, 2005)

The BBB is originally described as the mechanical barrier that separates the circulatory system from the CNS and has been attributed to the formation of tight junctions between the endothelial cells of the brain microvasculature (Reese and Karnovsky, 1967). In these tight junctions, claudin and occludin proteins interact to each other and form an impenetrable barrier between the blood circulation and the brain (Abbott et al., 2006). Further studies demonstrated that the BBB is not only a mechanical barrier, but it is also an active chemical and metabolic barrier. P-glycoprotein and multidrug resistance-associated proteins actively exclude compounds from the brain. (Zlokovic et al., 2008). Moreover, the cells of the BBB express high levels of metabolizing enzymes such as cytochrome P450 family (Minn et al., 1991). These barriers all contribute to the function of the BBB. From the properties described above, it has been postulated that BBB penetration requires a drug to have none of the following: a molecular weight greater than 500 Daltons, more than 10 hydrogen bond donors/acceptors, affinity for the BBB enzyme system, affinity for the BBB efflux system, or high binding to plasma proteins (Pardridge, 2002). BBB poses a direct barrier between the CNS and systemic circulation, therefore, strategies to circumvent the BBB would be of greatest interest in the development of CNS drug delivery systems.

The blood–CSF barrier is the barrier between the systemic circulation and the cerebrospinal fluid. The blood–CSF barrier is similar to the BBB and can exclude chemicals from the CNS. It serves as a selective filter allowing some molecules pass through to form the cerebrospinal fluid. Tight junctions between the epithelial cells of the choroid plexus create the mechanical barrier. A characteristic of choroid plexus is that there are not tight junctions in the capillaries, but there are fenestrae between the capillaries that supply the region. Drug and other molecules can freely diffuse from the capillary through these fenestrae, but they are prevented from entering the CSF by the epithelial tight junctions. Another property of the blood–CSF barrier is the surface area relative to the BBB. The blood–CSF barrier has 1,000 times less surface area than the BBB, thus the blood–CSF barrier is a less significant obstacle to delivery (Pardridge, 1992).

One common overlooked obstacle to CNS delivery is the dilution effects and metabolism/degradation due to systemic distribution and clearance of drugs in peripheral tissues. Previous works have employed the approach of increasing lipophilicity of drug molecules for increasing CNS permeability, however, these lipophilic compounds became more readily penetrate into all other tissues when administered into the systemic blood circulation. With the increase in systemic distribution, a larger dose must be given to achieve the required therapeutic levels in

the CNS. This leads to non-specific systemic effects and increased systemic toxicity. Previous studies have stated that drug delivery to the CNS is difficult when the drug has high plasma protein binding affinity, as there is little free drug to diffuse into the CNS. In general, this is frequently considered a minor barrier to CNS delivery though, it is one area that could benefit tremendously by using novel drug delivery systems. For instance, the overall pharmacokinetic profile could be altered by encapsulating the therapeutic agent in a carrier (Warren et al., 2018).

37/67 KDa Laminin Receptor (LamR)

Cell membrane isolated $LamR^{67}$ binds native laminin purified from Engelbreth Holm Swarm murine sarcoma with 2nM K_d affinity (Malinoff & Wicha, 1983; Rao et al., 1983). On the other hand, *E. coli* expressed and purified recombinant $LamR^{37}$ showed a 700nM affinity of binding to laminin-1 (Jamieson et al., 2008; Zidane et al., 2013). The other study compared the binding affinity between LamR and Laminin, it indicated a similar K_d of 300~400nM for both 37 and 67 species, by using surface plasmon resonance (Fatehullah et al., 2010). Although it's still unclear for the binding mechanism between LamR and laminin, four putative binding sites including peptide G (residues 161-180), direct binding region (205-229), five separate x(D/E)W(S/T) repeats in the c-terminal and a motif consisted of Phe-32, Glu-35, and Arg-155, on LamR have been indicated to associate with laminin. Another Report also suggested that the N-terminal (1-220) and C-terminal (225-295) of LamR can independently bind laminin-1, implying these putative binding site work individually. Interesting, some of the truncated LamR proteins are shown to be capable of binding laminin and heparan sulfate (HS) simultaneously, while full length LamR37 and LamR67 are seemingly incapable of binding or weakly bind to HS (Guo et al., 1992; Kazmin et al., 2000).

Through the binding with laminin, LamR also participate for certain modes of cellular adhesion and migration (Chen et al., 2009; Poon et al., 2011; Venticinque et al., 2011). In additional to serving as laminin binding receptor, LamR is also well known as a structural component of the ribosome. Research has shown that LamR37 associates with the 40S small subunit of ribosome (Anger et al., 2013; Ben-Shem et al., 2011; Malygin et al., 2011; Scheiman et al., 2010a, b). The N-terminal of LamR is responsible for ribosome binding, as truncated LamR37 (1-220) can recover translation deficiency caused by LamR knockdown (Scheiman et al., 2010a). Beside the direct ribosomal function, LamR is critical for maturation of 21S pre-rRNA into 18S rRNA process which represents not only a ribosomal biogenesis activity of LamR but also a nucleolar function, as LamR is required for nucleolar exit of pre-40S subunit (O'Donohue et al., 2010).

The identity of LamR37/67 and the relationship between the lower and higher molecular weight species have been a research focus over the last four decades. However, no demonstrative conclusion has been drawn. LamR37 has been found in the nucleus (Scheiman et al., 2010a), in the cytosol, associated with the cytoskeleton, associated with ribosomes and in the plasma membrane. LamR67 is presumed to be somehow derived from LamR37, but the actual identity of this protein remains unclear. The most popular hypothesis is that LamR67 is a heteromeric protein consisted by LamR37 and some galectin family protein since previous studies have proved cross reaction with LamR67 by anti-lectin antibody.

The past studies indicated that LamR67 is the major form located at the plasma membrane (Fujimura et al., 2005) and the membrane abundances of both LamR37 and LamR67 are significantly less than the overall cytoplasmic level. While antibody against epitopes in N-terminal of LamR only detect the protein with cell permeabilization, C-terminal-directed antibodies are capable of labelling LamR on the cell surface without cell permeabilization (Castronovo et al., 1991). However, the LamR37 (9-205) crystal structure shown no apparent transmembrane domain and the membrane targeting signal peptide is neither unlikely, while a prediction of an atypical and short transmembrane domain within residue 86-101 of LamR37 would result in some 100 intracellular N-terminal residues (Rao et al., 1989). Although definitive evidence is lacking, two hypotheses for LamR membrane association have been supported by numerous reports. First, the association could occur through a hydrophobic region of LamR37 or a modification, a mechanism of adhesion common for exoplasmic peripheral membrane proteins. Second, LamR associates with other protein and thus adherent to the cell membrane.

Introduction

The blood-brain barrier (BBB), blood-spinal cord barrier (BSCB) and dilution effects due to the systemic distribution limits the development of promising therapeutics to treat CNS diseases, such as amyotrophic lateral sclerosis (ALS), Alzheimer's disease (AD), Parkinson disease (PD), and spinal muscular atrophy (SMA) (Barchet and Amiji, 2009; Dong, 2018). Previous reportS have estimated that as many as 1.5 billion people are suffered from some type of CNS disorder at any given time, worldwide (Federoff, 1999). In 2016, neurological disorders were the leading cause of disability and the second leading cause of death (Feign et al., 2019). Moreover, the absolute number of people affected by, dying, or remaining disabled from neurological diseases over the past 30 years has been increasing globally and is expected to be continually increased in the future, driven to a considerable extent by the aging of population (GBD 2016 Neurology Collaborators, 2016). For instance, about 1 out of 65 people are diagnosed with AD in the U.S. every year and the percentage were expected to triple by the mid-21st century (Vega et al., 2017). 1-2 out of 1000 people in the U.S. develop PD (Tysnes and Storstein, 2017) and the number was estimated to double by 2040 (Rossi et al., 2018). 5-7 out of 100,000 people in North American have Huntington's disease (Pringsheim et al., 2012). Thus, a significant unmet need for promising CNS disease treatments and drug delivery methods exists.

In the past, researchers have developed a variety of approaches for overcoming the barriers to CNS delivery, such as invasive methods including intracranial delivery and transient BBB disruption via chemical or focused ultrasound (Bloch et al., 2004; Burgess et al., 2013; Zünkeler et al., 1996). Other attempts were addressed to enhance the bioavailability of molecules through non-invasive strategies. For example, some nano-sized carriers including liposome, solid-lipid nanoparticles and polymeric nanoparticle were designed to effectively package the therapeutics and enhance the transport across BBB. (Huwyler et al., 1996; Lockman et al., 2003; Sun et al., 2004) Also, biologics such as adeno-associated virus (AAV)-based, antibody-based and peptide-based delivery have been developed and proved to mobilize chemicals, proteins, genes or siRNAs into CNS (Ahlschwede et al., 2019; Federici and Boulis, 2006; Gray et al., 2013; Spencer and Verma, 2007; Wu et al., 2019; Yu et al., 2011; Zhou et al., 2011). To Successfully deliver target therapeutics to CNS while avoiding extensive systemic distribution, the transporters and receptors that actively transport compounds in and out of the CNS were investigated and acted as the delivery target. Through some chemical modifications, the therapeutics and delivery agents could increase their affinity to influx transporter/receptors for enhanced CNS delivery, or decrease its

affinity to efflux transporter for better CNS retention. One instance successfully adopted this approach in clinical is levodopa, a dopamine precursor, it's penetration into the CNS is enhanced by the 4F2hc/LAT1 complex (Kageyama et al., 2000). By using known CNS delivery agent and modifying it to make it chemically resemble a naturally transported molecule or increasing the valence of delivery agent, enhanced CNS penetration occurs (Tsuji and Tamai, 1999).

Our lab previously developed a strategy to screen bacteriophage display libraries in mice and identified a targeted axonal import (TAxI) peptide which enabled the accumulation of recombinant M13 bacteriophage into the spinal cord via somatic motor neurons that projected to peripheral neuromuscular junctions. Through intramuscular (IM) injection, synthesized TAxI peptide could traffic and deliver functional enzymes into spinal cord motor neuron via motor axon which projected to periphery in mice. TAxI delivery into motor neurons after peripheral administration was repressed in animals underwent unilateral L1-L4 rhizotomy which caused transected peripheral nerve roots, indicating that TAxI was delivered to CNS via a retrograde axonal transport mechanism. For quantification, TAxI and a positive control peptide, transactivator of transcription (TAT) peptide (Nagahara et al., 1998) were complexed with NeutrAvidin horseradish peroxidase (NA-HRP) and administered by IM injection. TAxI was mobilized to the spinal cord and the lumbar aspects of the cord over 4.5-fold and 18-fold over the TAT peptide, respectively. Moreover, TAxI peptide was demonstrated to label motor neuron in human spinal tissue. These results suggested that TAxI-mediated delivery was an effective and non-invasive approach for the transportation of macromolecular therapeutics to CNS through peripheral administration. (Sellers et al., 2016).

Another following study from our lab has also demonstrated the potential to utilize different targeted ANS-to-CNS uptake ligands, or TACL peptides to enhance delivery to different regions to the CNS through IP injection. While TACL increased protein delivery into the spinal cord and forebrain, however, TAxI strongly enhanced protein distribution in spinal cord and hindbrain, suggested preferable or alternate selective routes of delivery through ANS, for example, via sympathetic or parasympathetic neurons routes, for different peptides. Through decafluorobiphenyl (DFBP) modification, the serum stability, resistance to degradation and target binding affinity were significantly improve against peptides stabilized by disulfides, amides, or triazoles formed by click cyclization chemistry. To be specific, DFBP stapled TAxI peptide was proved to enhance in delivery to hindbrain and labelling in ANS neurons. Animals

injected with a micromolar drug dose by IP, show picomolar levels of drug activity in the CNS. (Sellers et al., 2019)

To further improve the affinity and understand the delivery mechanism involved with the mobilization of TAxI into CNS, we employed approaches such as peptide sequence optimization and synthesizing multivalent binder via the N-(2-Hydroxypropyl) methacrylamide (HPMA) polymer conjugation. For sequence optimization, we incorporated the part of the sequence which was found to be responsible for CNS penetration, on the loop A motif of capsid protein from adeno-associated virus 9 (Choudhury et al., 2016), on the N-terminal of the original TAxI peptide. On the other hand, many reports have demonstrated that affinity peptides can be conjugated on polymer to yield multivalent binders with enhanced affinity to their target receptors (Jeong et al., 2018). Furthermore, multivalent binding derived retention, endocytosis and intracellular trafficking have been reported and proved to be beneficial for CNS delivery (Ficther et al., 2008; Lin and Anseth, 2009; Radford et al., 2020). Among the available polymer scaffolds, the characteristic and functionality of HPMA based co-polymers have been well-studied. Besides, HPMA polymerization is advantageous over other methods for peptide-polymer conjugation. For instance, the technique was employed as a well-controlled facile method of synthesis with high yield of final product (Johnson et al., 2011). The peptide HPMA-copolymers were generally found to be stable in the extracellular matrix (ECM) and they can be engineered to be biodegradable by using environmentally responsive elements (Shi et al., 2013). Most importantly, by varying ligand density on HPMA copolymers, the increasing of target binding affinity/avidity were observed through the effect of multivalency on targeting capability (Chu et al., 2013; Ngambenjawong and Pun, 2017). Recently, a pull-down assay and mass spectrometry result revealed that human laminin receptor (hLamR) could be a potential binding target for TAxI peptide (Sellers et al., unpublished data). However, solid evidence for the binding between TAxI and hLamR is still lacking and the affinity is required to be measured and optimized.

The 37/67 kDa Laminin Receptor (LamR), or the ribosomal protein SA (RSPA) is a multifunction protein which localizes in nucleus, cytoplasm, ribosome, plasma membrane and ECM to exert different functions such as laminin binding, protein translation, cytoskeletal organization, nuclear function and cell signaling (DiGiacomo and Meruelo, 2016). LamR has been shown to have remarkably diverse physiological roles and little is conclusive about the regular physiological area and the various higher molecular weight species of LamR in cells. However, the function of laminin binding is the most studied and fundamental aspect of LamR. To date, a definitive crystal

structure of LamR or the four putative binding sites on LamR has not been published to detail how LamR associates with laminin. Thus, researchers do not have a definitive model to detail how LamR binds laminin. However, binding studies have demonstrated that LamR participates and facilitates cellular adhesion and migration. Moreover, LamR has been shown to promote cancer invasion and metastasis (Chen et al., 2009; Poon et al., 2011; Venticinque et al., 2011). Moreover, several clinical and nonclinical reports have been demonstrated that LamR-overexpression in multiple types of cancer correlates with disease progression (Berno et al., 2005; Givant-Horwitz et al., 2004; Kumazoe et al., 2013). Previous studies have also investigated the possibility of using LamR as a onco-target for cancer therapeutics or delivery (Pesapane et al., 2015; Umbaugh et al., 2017). Nonetheless, LamR has the potential to serve as a ligand receptor on cell membrane for target therapeutics and cargo delivery.

Interestingly, TAxI was found to enrich in the environment with abundant of proteoglycans (PGs) in the ECM of CNS. PG is a huge heterogeneous group of extensively glycosylated proteins which comprise a core protein and one or more covalently bonded glycosaminoglycans (GAGs). Based on the nature of GAGs on the core protein, PGs are classified into several distinct group, for instance, they generally have a single type of GAG chain such as chondroitin sulfate (CS), heparan sulfate (HS), or dermatan sulfate (DS) on serine residue of the core protein and are categorized as CSPGs, HSPGs or DSPGs accordingly. Previous studies have been demonstrated PGs located in the ECM or on the outer surface of cell could function as a receptor, co-receptor, or co-factor for several ligands or ligand/receptor association (Dyck and Karimi-Abdolrezaee, 2015). For example, CSPGs have been reported as co-factor for the interaction between AMPA and kainate receptor (Maroto et al., 2013). Moreover, 95% of cancer modified their glycocalyx, in particular, they significantly overexpressed PGs to strength cell adhesion, interact with receptor on the cell membrane and change their activities (Kanyo et al., 2020). Therefore, PGs potentially participate by certain ways in TAxI-based target delivery.

Here, we report TAxI binds to cells that express hLamR on the surface and demonstrate correlation binding between TAxI and hLamR. Through peptide sequence change, a TAxI-based peptide monomer slightly increases affinity to hLamR. A multivalent TAxI-HPMA co-polymer further enhanced LamR-binding, especially in cells with high LamR expression. TAxI shows a robust association to cancer cells and weak binding to non-cancer cells. Moreover, we conclude that CS is an allosteric modulator which promotes the interaction between TAxI and hLamR. In addition, the development and optimization of a process for eukaryotic recombinant hLamR protein expression and

purification is presented. In summary, TAxI peptide was engineered for enhanced target binding to potentially increase therapeutics delivery to CNS or certain types of cancer through the target receptor hLamR.

Materials and Methods

Flow Cytometry

Binding Assay

cells were lifted by versene solution (Gibco™, 1504006), collected, spin-downed at 500xg for 3-5mins and resuspended in 1mL HBSS (Gibco™, 24020117). Take cells sufficient for $2.5x10^5$ cells per 96-well and wash the cells in at least 5mL HBSS to remove FBS from media, then spin-down at 500xg for 3-5mins. Aspirate supernatant and add 1:500 Zombie Violet (Biolegend, 423113) in HBSS (volume depends on cell numbers, need 100uL per $1x10^6$ cells, e.g. add 500µL HBSS and 1uL Zombie Violet for 5 $x10^6$ cells) to resuspend and stain for 15 mins at room temperature, protected from light. Spin down the cells at 500xg for 5 min at room temperature, aspirate supernatant, and resuspend cells in staining solution (HBSS with 1% BSA, freshly-make) at $1.25x10^6$/mL. Aliquot 200µL ($2.5x10^5$ cells) per well of a 96-well round-bottom plate. Spin down plate at 500xg for 3min at room temperature, flick off supernatant, and resuspend cells in 100µL staining solution with appropriate amount of peptide. Make serial 1:2 dilutions of binding solution for eleven to twelve different concentrations of peptide, which spans two to three logs of concentration. Include an unstained group as a control streptavidin only group, and gating group. Incubate for 30-60mins at 4℃ protected from light. Spin the plate at 500xg for 3 min at 4℃, flick off supernatant, and resuspend wells with 200uL TBS with 1% BSA, and repeat this step once. Spin down plate at 500xg for 3 min at 4℃ and flick off supernatant, for biotinylated peptides, resuspend cells in 100uL stain solution (1:1000 fluorescent streptavidin). Alexa Fluor® 647 Streptavidin (Biolegend, 405237) was used, incubated 15-30 mins at 4℃ protected from light. Spin the plate at 500xg for 3 min at 4℃, flick off supernatant, and wash wells with 200 uL TBST with 1% BSA, and repeat this step once. Spin the plate at 500xg for 3 min at 4℃, flick off the supernatant, and resuspend cells in 200 µL PBS. Run FACS on the samples using the Attune NxT flow cytometry (ThermoFisher). Voltage settings are listed below, FSC: 60, SSC: 320, RL1: 250, VL1: 200. Acquire the mean fluorescent intensity (MFI) of each data point by FlowJo analysis software. Subtract the MFI of streptavidin only group to each data point. Plot the percent MFI for each concentration to create the binding curve and analyze affinity (Kd) by performing a non-linear curvefit (one site, specific binding with Hill slope) with GraphPad Prism.

Correlation Analysis

The initial procedures are the same as the method described above for binding assay, extra non-Zombie Violet (ZV) stained ells are needed. After aliquoting cells to 96-well round-bottom plate, spinning down and flicking off, resuspend cells in 100 µL staining

solution with groups listed below in both non-ZV cells: unstained control, TAxI peptide staining only and hLamR Antibody (Abcam, ab133645) staining only; also resuspend cells in 100 µL staining solution with groups listed below in ZV-prestaining cells: ZV stained only, TAxI peptide staining, Scrm peptide staining, TAxI and hLamR co-staining and Scrm and hLamR co-staining. Incubate for 30-60 mins at 4℃ protected from light. Spin down plate at 500xg for 3 min at 4℃, flick off supernatant, and resuspend wells with 200uL TBS with 2% BSA and 1:100 yeast tRNA (Invitrogen, AM7119), and repeat this step once. Spin down plate at 500xg for 3min at 4℃ and flick off supernatant, resuspend cells in 100uL stain solution with appropriate fluorescent streptavidin, secondary antibody or both, including 1:1000 Alexa Fluor® 647 Streptavidin (Biolegend, 405237), 1:800 Alexa Fluor® 488 AffiniPure Donkey Anti-Rabbit IgG (JacksonImmunoResearch Labortories, 711-545-152), incubated 15-30mins at 4℃ protected from light. Spin down plate at 500xg for 3min at 4℃, flick off supernatant, and wash wells with 200uL TBST with 1% BSA, and repeat this step once. Spin down plate at 500xg for 3min at 4℃, flick off supernatant, and resuspend cells in 200µL PBS. Run the samples on Attune NxT flow cytometry (ThermoFisher). Voltage settings are listed below, FSC: 60, SSC: 320, RL1: 250, BL1:300, VL1: 200. The single-stained cells are used for compensation in FlowJo, the rest are plot by quadrant dot plots for analysis.

Antibody staining

The cells were lifted by versine solution (Gibco™, 1504006) or PBS, depends on cell types, collected, spin-downed at 500xg for 3-5mins and resuspended in 1mL PBS. Take cells sufficient for $2.5x10^5$ cells per 96-well and wash the cells in at least 5mL PBS to remove FBS from media, then spin-down at 500xg for 3-5mins. Spin down cells at 500xg for 5min at room temperature, aspirate supernatant, and resuspend cells in PBS with 1% BSA at $1.25x10^6$/mL. Aliquot 200µL ($2.5x10^5$ cells) per well of a 96-well round-bottom plate. Spin down plate at 500xg (Can go as high as 750xg spins if your cells are difficult to pellet) for 3min at room temperature and flick off supernatant. For intracellular detection, resuspend the cells by 100µL Fixation/Permeabilization solution (BD, 554714), incubate at 4℃ for 20mins, then spin down plate at 500xg (750xg is recommended for cells fixed and permed hereafter) for 3mins at 4℃ and flick off supernatant (skip this step for surface detection). Resuspend cells with 200uL TBS with 1% BSA, spin down and flick off, then repeat this step once. Resuspend cells in 100uL hLamR antibody solution (1:100 in PBS with 1% BSA for surface detection or in BD's Perm/Wash™ Buffer for intracellular detection, use respective buffers for all the wash and staining hereafter). Incubate for 30-60mins at 4℃ protected from light. Spin down plate at 500xg for 3min at 4℃, flick off supernatant, and resuspend wells with 200uL

respective buffers, and repeat this step once. Spin down plate at 500xg for 3min at 4℃ and flick off supernatant, resuspend cells in 100uL secondary antibody solution (1:800 of Alexa Fluor® 488 AffiniPure Donkey Anti-Rabbit IgG in the respective buffers, incubated 15-30mins at 4℃ protected from light. Spin down plate at 500xg for 3min at 4℃, flick off supernatant, and wash wells with 200uL TBST with 1% BSA or BD's Perm/Wash™ Buffer, and repeat this step once. Spin down plate at 500xg for 3min at 4℃, flick off supernatant, and resuspend cells in 200μL PBS with 0.1% PFA. Run the samples on Attune NxT flow cytometry (ThermoFisher). Voltage settings are listed below, FSC: 60, SSC: 320, RL1: 250, BL1:300, VL1: 200.

Cell Culture

HeLa and HepG2 cells were cultured in RPMI 1640 medium supplemented with 10% fetal bovine albumin and antibiotics (100 U/ml penicillin and 100 μg/ml streptomycin). GBM8 cells were cultured in DMEM/F-12 medium supplemented with B27 (1X), heparin (5 mg/ml), GlutaMAX (1X), N2, Epidermal growth factor (20 ng/ml) and Fibroblast growth factor (2 ng/ml). HEK293T cells were cultured in DMEM medium supplemented with 10% fetal bovine albumin and antibiotics (100 U/ml penicillin and 100 μg/ml streptomycin). These cells were incubated in a humidified incubator in 5% CO2 at 37℃.

Chondroitinase Treatment

Cells were first lifted by versene solution (Gibco™, 1504006) and spun down at 500xg for 3 mins to collect cells, then cells were washed with HBSS once. Spin down at 500xg for 3 mins and aspirate the supernatant, then resuspend cells in 0.5U/mL Chondroitinase ABC (Sigma-Aldrich, C2905) solution in 20mM HEPES, 0.02% BSA HBSS and incubate for 1hr at 37℃. Spin down at 500xg for 3mis and aspirate the supernatant, then wash cells with HBSS twice. Resuspend cells in 1% BSA HBSS at appropriate amount. ChABC treated cells were stained with anti-aggrecan (CS-56) antibody, anti-NG2 antibody, or incubated with TAxI peptide in different concentration of CS solution.

Cell Viability Assay

$1x10^4$ HEK293-T cells were seeded in 96-well plate per well. After 16 hours, DMEM medium were changed to DMEM medium containing 0, 0.3125, 0.625, 1.25, 2.5, 5, 10 and 20 μg/mL of puromycin. Continuing culture for 48 hours before adding 1/10 volume of AlamarBlue cell viability reagent (DAL1025, Invitrogen) directly into culture well. Incubate for 1 hour at 37℃ in the cell culture incubator, protected from light. Read fluorescence by excitation wavelength of 560nm and an emission of 590nm.

Transfection

HEK293T cells were seeded in 6 well plate. Transfection was initiated when cells reached to about 80% confluency. Two transfection reagents have been used. By using Lipofectamine 2000 (), first dilute appropriate amount of lipofectamine reagent and DNA in Opti-MEM () medium, respectively. Combine diluted lipofectamine reagent and diluted DNA by a ratio of 1:1. Incubate for 5 minutes at room temperature. Gently add DNA-lipid complex to the cells and incubate overnight. By Using BioT, dilute DNA and BioT reagent in DPBS. Pipeting up and down the mixture a few times and leave at room temperature for 5 minutes. Gently add entire mixture to cells and incubate overnight.

Transduction

Aliquot $4x10^5$ HEK293-T cells in 500µL completed growth medium. Add polybrene and lentivirus at desired MOI to 100µL completed growth medium and incubate 5 minutes at room temperature. Gently mix cells and lentivirus preparation. Seed the cell and virus mixture to 6-well plate. Allow the cell to grow for 24 to 48 hours before selection.

Virus Tittering

HEK293-T cells were transduced with 1:10 serial diluted lentivirus, from 1:10,000, 1:100,000 to 1:1,000,000, respectively, in 6-well plate. 2.5µg/mL puromycin was added to each well.

Protein Extraction

For western blotting, add RIPA buffer (Thermo Scientific™, 89900) with 1mM PMSF (added before use) and EDTA-free protease inhibitor cocktail (Roche, 11873580001) to harvested cell pellet. Vortex and incubate on ice for 20 to 30 minutes. Centrifuge at 18,000 x g at 4°C for 20 minutes. Take supernatant to new microcentrifuge tube.

SDS-PAGE

The cell extracts were mixed with Laemmli Sample Buffer (Bio-Rad, 1610737) and heated at 95°C for 6mins. Then the protein samples were loaded into 4 to 20% Tris-Glycone Mini Protein Gel (Invitrogen™, XP04200BOX) in electrophoresis tank filled with 1x Running Buffer (25mM Tris-base, 190mM glycine, 0.1% SDS). Run the gel at 100V for 20mins, then gradually increase to 220V until the loading dye migrate off the gel.

Coomassie Blue Staining

After SDS-PAGE, rinse the gel three times on the shaker with nano-pure H2O for 5mins each at room temperature. Flick off H2O and stain the gel with Coomassie Blue staining solution for 1hr at room temperature on the shaker. Flick off staining solution and wash at least 3 times (or until the proper background is gained and protein bands are visible).

Western Blotting

After SDS-PAGE, proteins were transferred from the gel to PVDF membrane. PVDF membrane was first pre-active by soaking in methanol for at least 15 seconds. The transfer cassette sandwich was prepared as below. Place the cassette, with the black side down, in the blotting tray. Fill the bottom of both segments of the tray with 1x Transfer Buffer (25mM Tris-base, 190mM glycine, 20% methanol, 0.1% SDS). Prewet a fiber pad in the first segment of the tray and place on the black side of the cassette. Prewet a filter paper and place on the fiber pad. Place the equilibrated gel on the filter paper with the cut off corner in the top right. You can grab the gel from the bottom using your fingers to do this. Use a roller to remove any bubbles and to spread out gel. Place the equilibrated membrane on the gel such that the cut off corners align (use tweezers). Use a roller to remove any bubbles. Prewet the last filter paper and complete the sandwich by placing it on membrane. Use a roller to help complete the sandwich. Prewet the last fiber pad and add to the filter paper. Close the cassette firmly but carefully, locking it closed with the white latch. Place the cassette in the module with the white latch facing up and with the black side facing the black part of the module. Then transferring in the tank filled with 1x Transfer Buffer at 50V for 3hrs. Rinse the membrane with TBST, and block the membrane with TBST 3% BSA on the rocker/shaker at room temperature for 1hr. Flick off blocking solution and rinse the membrane twice with TBST for 5 mins each on the rocker/shaker at room temperature. Flick off TBST and incubate the membrane with primary antibody in TBST 1% BSA on the rocker/shaker for overnight at 4°C. On the Second day, flick off solution and wash three times with TBST twice on the shaker for 5mins each at room temperature. Flick off TBST and incubate with appropriate secondary antibody on the shaker for 1hr at room temperature. Flick off solution and wash three times with TBST twice on the shaker for 5mins each at room temperature. Flick off TBST and incubate with ECL HRP substrate (Thermo Scientific™, 34580) for 3-5 mins at room temperature. Imaging on Xenogen IVIS 200.
Primary antibody used: 1:1000 anti-hLamR (Abcam, ab137388); 1:1000 anti-6-His-Epitope Tag (Biolegend, 906101); 1:1000 anti-GAPDH (Cell Signaling, D4C6R)
Secondary antibody used: 1:5000 goat anti-rabbit IgG (Sigma, A6154), 1:10000 goat anti-mouse IgG (JacksonImmuno Research Labortories, 115-035-174), NeutrAvidin™-HRP (Thermo Scientific™, 31030)

Protein Purification

Equilibrate column(s) to 4℃. Prepare sample by mixing the protein extract with an equal volume of Equilibration Buffer. Use the Equilibration Buffer to adjust the total volume to be ≥ 2 resin-bed volumes. Remove the bottom tab from the HisPur Ni-NTA 3mL Spin Column and place column into a 50mL centrifuge tube. Centrifuge column at 700 × *g* for 2 minutes at 4℃ to remove storage buffer. Equilibrate column with two resin-bed volumes of Equilibration Buffer. Allow buffer to enter the resin bed. Centrifuge column at 700 × *g* for 2 minutes at 4℃ to remove buffer. Place the bottom plug in the column and add the prepared protein extract. Mix on an orbital shaker or end-over-end mixer for 1hr at 4℃, perform multiple applications and centrifugations until the entire sample has been processed if the sample volume is greater than the column. Remove the bottom plug. Centrifuge the column at 700 × *g* for 2 minutes at 4℃ and collect the flow through in a centrifuge tube. Wash resin with two resin-bed volumes of Wash Buffer with 1% tween on an orbital shaker or end-over-end mixer for 15 mins at 4℃, then centrifuge at 700 × *g* for 2 minutes at 4℃ and collect fraction in a centrifuge tube. Repeat this step twice, first with Wash Buffer with 1% tween then without tween. Elute His-tagged proteins from the resin by adding one resin-bed volume of Elution Buffer. Centrifuge at 700 × *g* for 2 minutes at 4℃. Repeat this step two more times, collecting each fraction in a separate tube. Concentration the elution fraction by Amicon® Ultra-15 Centrifugal Filter Unit-10KDa cutoff (Millipore, UFC9010). Analyze all the fractions by SDS-PAGE and Coomassie Blue Staining.

Plasmid Preparation

For mini-prep, E. coli were cultured at 250rpm in 5mL LB with appropriate antibiotic (100μg/mL Ampicillin) in plastic culture tube for overnight at 37c. Resuspend pelleted bacterial cells in 250 μl Buffer P1 and transfer to a microcentrifuge tube. Add 250 μl Buffer P2 and mix thoroughly by inverting the tube 4–6 times. Add 350 μl Buffer N3. Mix immediately and thoroughly by inverting the tube 4–6 times. Centrifuge for 10 min at 17,900 x g. Apply 800 μl of the supernatant to the QIAprep 2.0 Spin Column. Wash QIAprep 2.0 Spin Column by adding 0.75 ml Buffer PE and centrifuging for 30–60 s. Discard the flow through, and centrifuge at full speed for an additional 1 min to remove residual wash buffer. Place the QIAprep 2.0 Spin Column in a clean 1.5 ml microcentrifuge tube. To elute DNA, add 50 μl Buffer EB (10 mM Tris·Cl, pH 8.5) to the center of each QIAprep 2.0 Spin Column, let stand for 1 min, and centrifuge for 1 min. For Max-prep,

Plasmid Construction

1. pLV-EF1a-hLamR-IRES-Puro

pLV-EF1a-IRES-Puro vector (bp) and synthesized 6xhis tagged hLamR fragment (bp) were co-digested by BamHI and EcoRI for 1 hour at 37℃, respectively. Both the cutted pLV-EF1a-IRES-Puro vector and cutted 6xhis tagged hLamR sequence were collected by gel extraction (). Ligate pLV-EF1a-IRES-Puro vector (30 ng) and cutted 6xhis tagged hLamR sequence with 1:3 molar ratio with 1μL T4 DNA ligase, 1μL 10x ligase buffer, and H2O up volume to 10μL, incubate overnight at 4℃.

2. pRSETb-hLamR
   pRSETb vector (bp) and PCR amplified hLamR fragment (bp) were co-digested by BamHI and EcoRI for 1 hour at 37℃, respectively. Both the cutted pRSETb vector and cutted hLamR sequence were collected by gel extraction (). Ligate pRSETb vector (30 ng) and cutted hLamR sequence with 1:3 molar ratio with 1μL T4 DNA ligase, 1μL 10x ligase buffer, and H2O up volume to 10 μL, incubate overnight at 4℃.
   Forward primer: 5'-AACACCAGGATCCGGAGGAAGCGGAGCTCTGG-3'
   Reverse primer: 5'-AATTATAGAATTCTCAGCTCCAGTCTGTGGTAG-3'

Transformation

Thaw Stbl2 competent cells (Invitrogen™, 10268019) on ice. Gently mix the cells, then aliquot appropriate amounts of competent cells into chilled tubes containing DNA ligation solution. Moving the pipette through the cells while dispensing. Incubate the cells on ice for 20 minutes. Heat-shock the cells 45 seconds in a 42°C water bath. Place on the cells ice for 3 minutes for recovery. Add 1 mL of LB and incubate at 37℃ for 1 hour. Centrifuge at 8,000 rpm for 1.5 min. Pour the supernatant and use the excess of supernatant to resuspend the pellet. Spread the cell solution on LB ampicillin plate and incubate 14-16 hours at 37℃.

Polymerase Chain Reaction (PCR)

5 ng or 10 ng of DNA template was added for 10μL or 50μL reaction, respectively, in addition to 1μM of forward and reverse primers, appropriate amount of master mix (), and H2O up volume to 10μL or 50μL. For the thermocycler, set a program as 95℃ for 3mins; 35 cycles of 95℃ for 30 seconds, specific annealing temperature for 30 seconds and 72℃ for 1 min; 72℃ for 8 mins; 12℃ hold.

Agarose Gel Electrophoresis

Prepare 1% agarose in 1xTAE buffer and add/mix 1:10000 ethidium bromide (). After solidification in the gel making cassette, put the gel in the running box filled with 0.5xTAE buffer. Run the gel with 130V for 20-30mins until loading dye is closed to the

bottom of the gel or migrate off. Put the gel on the UV light box and observe the result.

Solid Phase Peptide Synthesis (SPPS)

Weight proper amounts of amino acids and rink amide resin, then dissolve and vortex amino acids in the proper volumes of dimethylformamide (DMF) per the calculations by the software. Rinse the resin down by 50% DMF/50% Dichloromethane (DCM). Load newly made amino acid solutions, 1M N,N'-Diisopropylcarbodiimide (DIC), ethyl cyanohydroxyiminoacetate (oxyma), 20% piperidine onto the designated positions on Liberty Blue H12, and resin onto Liberty Blue H12, then run the synthesizer. After synthesis is completed, place and press tight a round filter on the bottom of 15mL Resprep column, then place the column on the aspirator in chemical hood, rinse the resins containing peptide products down into the column by DCM to swell and activate the resins (if not going to react immediately, rinse down by methanol and dry down). For methacrylamide (MA)-conjugated peptides, exchange the solution from DCM to DCM/3 equals NHSMA/3 equals 1-Ethyl-3-(3-dimethylaminopropyl)carbodiimide (EDC)/8 equals Triethylamine (TEA). Incubate on the end-to-end mixer for overnight at room temperature. Rinse with DCM 3 times, and cleave the peptides off the resins by 5% 1,4-Dimethoxybenzene (DMB), 2.5% Triisopropylsilane (TIPS), 2.5% 1,2-Ethanedithiol (EDT), 0.5% H2O and 89.5% Trifluoroacetic acid (TFA). Cleave for 3-4 hrs with 5mL cleavage solution for full-cleavage and 1 hr with 100uL for micro-cleavage. Slowly drop cleaved peptide solution into 9 times volume of pre-cooled diethylether for precipitating the peptides. Mix and spin down at 4500xg for 5 mins at 4℃. Decant the either, open the lid and cover with Kimwipes paper, then dry in vacuum for overnight at room temperature. On the next day, crush the precipitated powders as fine as it can and add about 5mL methanol, dissolve the powders by vortex and sonication, or heat up to 80℃ (if necessary). Once the powders dissolved, precipitate with diethylether and dry out in vacuum overnight again. The peptide will be ready for HPLC on the next day.

TAxI peptide sequence: SACQSQSQMRCGGG

Scrm peptide sequence: SACSQMGRQSCGQG

A98 peptide sequence: NHQSDGTLAVPCQSQSQMRCGGK

A98-TAxI peptide sequence: NHQSDGTLAVPCQSQSQMRCGGK

MALDI-TOF

Mix 1μL matrix and 1μL untested sample on the metal plate, leave to dry or by heat gun. Load the metal plate to the plate compartment and wait the vacuum reach less than $1x10^{-6}$. Set up method, calibrate with standard and run the sample.

Results

TAxI and Poly-TAxI bind to HeLa cells via hLamR

In order to investigate the affinity between TAxI-based peptides and hLamR, we synthesized biotinylated TAxI-based peptides and their scramble (SCRM) forms by SPSS and confirmed the molecular weight of peptide via MALDI-TOF to make sure the proper compositions (Fig. S1A&B). These peptides were then used in individual platforms of binding assay including flow cytometry (FACS). In the cell-based flow cytometry assay, titrations of peptide solution supplemented with CS were incubated with cell lines which have been confirmed to have surface expression of hLamR, such as HeLa, HepG2 and GBM8 cells (Fig. 1B, 3B & 4C). In HeLa cells, TAxI showed an affinity of 7.64 ± 1.51μM to the cells, under the condition of having 500μM soluble CS in the buffer, while the SCRM peptide exhibited minimum binding (Fig. 1C&D). Moreover, to verify the hypothesis that increased valency, driven by HPMA-based multivalent binder, can lead to improved binding affinity between delivering agent and the target, we also tested the binding of HPMA-TAxI co-polymer (Poly-TAxI), which has approximately 3 to 4 TAxI peptides conjugated per polymer, to HeLa cells, and a slightly improved affinity of 4.34 ± 0.42μM by Poly-TAxI's labelling was measured (Fig. 1E&F). These results suggested that TAxI-based peptides bind to the cell which possess hLamR on the cell membrane under the existence of additional CS in the buffer. However, the direct evidence of interaction between TAxI and hLamR was not yet proved. Therefore, to examine whether the binding of TAxI to the cell was mediated by hLamR, we performed a correlation study by flow cytometry. Since HeLa cells have the most homogenized surface expression profile out of the three cell lines that we used (Fig. 2D), they were chosen as the platform for analyzing correlation between TAxI and hLamR. In a quadrant dot plot analysis, TAxI and anti-hLamR antibody were able to label 56.8% of AF-647 positive events (Fig. 2B) and 57.1% AF-488 positive events (Fig. 2E), respectively. While the co-staining of TAxI and anti-hLamR antibody caused a signal shift to 51.2% AF-488/AF-647 double positive event in Q2 and a strong correlation between TAxI and hLamR was observed (Fig. 2C&G), whereas co-staining of SCRM and anti-hLamR antibody was not observed with signal shift (Fig. 2F&H). Therefore, the result indicate that TAxI was able to target cells through the binding with hLamR.

TAxI-peptides bind to human brain cancer stem cells, and demonstrate increased affinity to Poly-TAxI

Next, we employed GBM8 cells, a human brain cancer stem cell line, for further evaluating the binding affinity of TAxI-based peptides to assess TAxI-based peptides

on human CNS derived cells. Interestingly, hLamR staining indicated two population of cells in terms of hLamR's expression in GBM8 cells (Fig. 3B). First, the population with fluorescent intensity located around 10^2 to 10^3 are defined as "the low hLamR expressors" (Green in Fig. 3B), whereas the population accounted as only 15%, with relative stronger fluorescent intensity, has a peak located between 10^3 to 10^4, which also represented the existence of high dimensional hLamR complex on their cell surface, are defined as "the high hLamR expressors" (Blue in Fig. 3B). TAxI-based peptides with 500μM of CS were incubated with GBM8 cells and the overall affinity (all cells) and affinities in both low and high hLamR expressors were measured. First, TAxI exhibited an overall affinity of 9.09 ± 0.73μM (Fig 3D, black line), a similar Kd of 8.426μM in the high hLamR expressors (Fig 3D, blue line), and minimal binding in the low hLamR expressors in the contrary (Fig 3D, green line). Next, A98-TAxI followed the same trend in TAxI's binding to GBM8 cells, except a higher affinity compared to TAxI, it showed an overall Kd of 6.4±0.36Mm to all cells (Fig. 3F, black line), Kd of 6.86μM in the high hLamR expressors (Fig. 3F, blue line), and minimal binding to the low hLamR expressors (Fig. 3F, green line). Lastly, the Poly-TAxI's affinities were also measured in GBM8 cells. The overall affinity for Poly-TAxI was 3.03 ± 0.35μM in all cells (Fig. 3H, black line). Interestingly, Poly-TAxI demonstrated about a two-fold increase of affinity, as 1.67μM, in the high hLamR expressors, who estimated to have high dimensional hLamR complexes on the cell surface (Fig. 3H, blue line). Likewise, a minimum binding was observed in the low hLamR expressors (Fig. 3H, green line). These results suggested either peptide sequence modification or polymerization for increasing the valence could enhance the TAxI-based peptides affinity to their target, hLamR. To be specific, advantage brought by polymerization was significant than A98 modification, as Poly-TAxI showed three-fold of overall binding to GBM8 cells and a further enhancement of binding in the high hLamR expressors, which often related to hLamR overexpression in cancer cells. We then hypothesize that if cancer cells often overexpressed hLamR, the affinity between TAxI and cancer cells would be higher than with normal cells. To investigate the idea, we used a human liver cancer cell line, HepG2 due to their high expression of hLamR in the cell membrane (Fig. 4C) and a human kidney cell line, HEK293-T, which only has marginal surface hLamR expression (Fig. 4D), to compare TAxI's binding in tumor and non-tumor cells. As the result, TAxI's affinities to HepG2 and HEK293-T are 8.65 ± 0.55μM (Fig. 4G, orange line) and 30.7 ± 4.16μM (Fig. 4G, Purple line), respectively, whereas the SCRM peptide showed low binding to both cell lines. These results indicated that TAxI-base peptides have a robust and relative stronger affinity to the cells which expressed high hLamR on the surface.

Chondroitin Sulfate is an allosteric modulator that increases the binding affinity of TAxI on hLamR

TAxI peptide was found to enrich in tissue surrounding by abundant CSPGs in ECM. PGs such as CSPGs, HSPGs and heparin are known as direct receptors or can mediate the binding of antibodies, peptides and other molecules (Park et al., 2017). In the very begin of this study, we found TAxI's affinity to cells could be increased by adding soluble CS, in the concentration-dependent fashion. In HeLa, TAxI showed affinity of 20.29 ± 2.89μM, 16.1 ± 1.43μM and 7.64 ± 1.51μM with 0, 50μM and 500μM additional CS, respectively (Fig. 5A). Similar trend was found in HepG2 cells, with the presence of 0, 50μM and 500μM additional CS, TAxI's affinities were 23.25±3.87, 17.35±2.24 and 8.65±0.55μM (Fig. S2). Next, to address whether TAxI's binding was specifically dependent on CS rather than other types of proteoglycans, we compared the binding of TAxI in GBM8 cells under the presence of additional added CS or HS. When 500μM of soluble CS was presented in the binding buffer, TAxI peptide showed a Kd of 9.09±0.73μM to the cells (Fig 5B, orange line). In contrast, it exhibited a Kd of 27.23μM under the presence of 5μM HS (Fig 5B, black line). The result implied that CS was potentially the specific co-factor for the binding between hLamR and TAxI peptide. To further validate the role of CSPG as a co-factor facilitating the interaction between TAxI and hLamR, we pre-treated the cells with 0.5U/mL Chondronitinase ABC (ChABC), then measure TAxI's binding to the cell under no CS or multiple concentrations of CS. First, the removal of GAGs chains in CSPG through ChABC treatment was confirmed by staining of anti-Aggrecan (CS-56) antibody, which has been reported to be specific for GAG portion of native CSPG. FACS result indicated that more than 90% and ~85% of GAGs of CSPG were digested in HeLa and GBM8, respectively (Fig. 5C&D). After ChABC treatment, TAxI showed Kd of approximately 31μM to both HeLa and GBM8 cells, when without CS in the binding buffer. However, a recovery of affinity was observed when the CS concentration gradually increased. In HeLa, TAxI's affinity to ChABC treated cells were 21.11, 16.42, 9.85, 8.49, 8.84 and 6.7μM when added 78μM, 156μM, 313μM, 625μM, 1.25mM and 2.5mM CS in the buffer, respectively (Fig. 5E). Similarly, with 78μM, 156μM, 313μM, 625μM, 1.25mM and 2.5mM CS, TAxI's affinities were measured as 14.57, 11.42, 9.4, 8.36, 6.98 and 6μM to ChABC treated GBM8 cells (Fig. 5F). In addition, all the data were fitted by allosteric modulation shift model and the α values were measure as 1.746 and 1.755 in HeLa and GBM8 cells, respectively, suggests CSPG has a positive cooperativity for binding between TAxI and hLamR. Thus, TAxI's affinity to hLamR was reduced due to the removal of GAGs in CSPG on the plasma membrane. Moreover, the additional soluble CS can recover the affinity lost causing by ChABC treatment. The results demonstrated that CSPG as a co-factor to facilitate the binding between TAxI and

hLamR.

Expression and purification of recombinant hLamR protein from HEK293-T cells

Previous reports have demonstrated the affinity tested between a pair of ligand and receptor could be different in orders and magnitudes via different assays (ref.). Moreover, since the cell surface and the surrounding ECM is a complicated environment, the non-cell based in vitro assay could further validate the predominant role of hLamR in TAxI peptide's binding and delivery. The rationales above suggested a benefit for measuring the kinetics via using purified hLamR protein and synthesized peptides in a noncell-based assay. In order to have sufficient amount of purified hLamR protein, lentivirus was used for making stable cell line. Lentiviral transfer plasmid was constructed by inserting a fragment featured by Kozak sequence, and sequentially followed by a 6xhis-tag, TEV sequence, and the full-length hLamR coding sequence, on the downstream of EF1a core promoter (Fig. 6A). The plasmid construct was verified by restriction enzyme digestion (Fig. 6B) and Sanger sequencing, then the plasmid was co-transfected with packaging plasmids and envelope plasmid into HEK293-T to produce virus particles. In order to understand the titer of lentivirus and acquire appropriate multiplicity of infection (MOI) for transduction, HEK293-T cells was transduced with 1:10 serial diluted lentivirus, then treated with 2.5μg of selection agent, puromycin, on the third day, the cells were continually incubated with puromycin containing medium for 6 days. As a result, $1:10^{-4}$ virus dilution showed a lawn which was not countable, whereas $1:10^{-5}$ and $1:10^{-6}$ have 402 and 55 colonies. We used 1.5 mL of puromycin containing DMEM to cover the well, thus the titer of virus could be counted as, $402/1.5*10^5 = 2.68x10^7$ and $55/1.5*10^6 = 3.67x10^7$. Therefore, the average transduction unit (TU)/mL was $3.175x10^7$ for the hLamR gene-carrying lentivirus (Fig. 6C). Since HEK293-T is a quick growing and virus transducible mammalian expression system with proper post-translational modification, we selected it as the recombinant protein expression platform. In the purpose of selecting a stable cell line which can consistently express the recombinant hLamR protein, we first tested the appropriate concentration of the selection agent used, puromycin, in HEK293-T for stable line selection. The kill curve indicated 48 hours incubation with puromycin over 1.25μg/mL could induce over 90% growth inhibition, in these concentrations, 2.5μg/mL was the lowest concentration which induced over 95% of death in untransduced HEK293-T cells. Therefore, we selected 2.5μg/mL of puromycin as the proper concentration for the other stable cell line making procedures (Fig. 6D). For making the recombinant His-tagged hLamR protein expressing stable HEK293-T cell line, we transduced HEK293T at MOI of 0.5, 1, 5 and 10, then selected the cells with 2.5μg/mL puromycin for 9-14 days before harvesting the cell lysates, a western blotting was conducted to determine

expression level of recombinant his-tagged hLamR protein in cells infected at different MOIs. The result suggested his-tagged hLamR are all overexpressed in the transduced cells. Predictably, the higher the MOI, the stronger the expression level. Within these groups, cells transduced at MOI 10 showed 5.67-fold of expression when comparing to the untransduced cells. The blotting of anti-his antibody revealed his-tag was properly expressed and again cells transduced at MOI 10 showed highest expression, as 1.66-fold compared to cells transduced at MOI 0.5, among the MOIs. His-tag was not detected in the untransduced cells (Fig. 6E). Since the cell transduced at MOI 10 has the best recombinant protein yield, it was stained with anti-hLamR antibody and ran on flow cytometer to confirming recombinant hLamR cellular location, the result indicated a slight increase of hLamR expression on the cell surface compared to naïve HEK-293T cell (Fig. 6F&4F). As the result, we successfully established a stable HEK293-T cell line expressing his-tagged hLamR for downstream assay and protein purification.

Process development for recombinant his-tagged hLamR purification

Ni-NTA resin (88226, Thermo Scientific) was used for purifying the recombinant his-tagged hLamR protein, a few rounds of buffer composition, incubation time and washing optimization were conducted initially. Among these, imidazole concentration in the buffers and pH level are the two main factors affecting the final product purity and yield. Because of the structure similarity, imidazole serves as the competitor to his-tagged protein for binding onto nickel resin, thus optimization on imidazole concentration in each step can greatly influence the successfulness of purification. Also, the working pH range of nickel resin is between pH 7 to 8. In theory, the higher pH condition comes with better product yield but also with higher non-specificity. The purpose of buffer and wash optimization is to find the balance between satisfactory yield of target recombinant protein and acceptable amounts of unspecific protein in the final product. In the beginning, multiple pH levels were tested, including pH 7.1, pH 7.6 **(Fig. 8A)** and pH 8.0 (data was not shown). As the result, no significant difference was observed in each step, thus all the buffers are pH 7.6 thereafter. Next, 10mM imidazole equilibration buffer and 50mM or 100mM imidazole wash buffers were used in the binding step and the washing step, respectively. **Fig. 8B** showed that a moderate yield of the 67KDa hLamR heterodimer (red square) and 37KDa hLamR monomer (red asterisk) were successfully eluted out of the Ni-NTA columns washed by 50mM imidazole wash buffer, while an unsatisfactory yield of hLamR protein was observed in the Ni-NTA column washed by 100mM imidazole, suggesting 50mM imidazole is better condition for washing. However, significant amounts of unspecific proteins were also eluted out in 50mM imidazole washed Ni-NTA column, especially apparent after concentration, this pointed out different washing method and stringent binding

environment for eliminating undesired proteins binding in the very beginning are needed. Thus, the comparison study between using 10mM and 30mM imidazole in the binding step was conducted subsequently. Also, in the previous rounds of purification, the Ni-NTA column were washed three times by merely adding wash buffer, flow-through and spun down to remove buffer. To address incomplete washing observed in previous rounds of purification, tween-20 was added into the wash buffer except the last round of wash and the wash buffer was mixed and incubated with the Ni-NTA column by end-over-end mixer for 15 minutes at 4℃, for each round of wash. Coomassie blue staining indicated successful elution of 67/37KDa hLamR proteins with some unspecific proteins in 10mM imidazole binding condition and successful elution of 67/37KDa hLamR proteins with very little of unspecific proteins in 30mM imidazole binding condition **(Fig. 8C)**. Moreover, wash time optimization study was conducted, the result dictated 4 times of wash after binding are the most appropriate for generating subtle balance between satisfactory yield and product specificity (Fig. 8D). Therefore, through the process optimization, we concluded that 30mM, 50mM and 300mM imidazole are the best condition for binding, washing and elution steps, respectively, in the Ni-NTA-based recombinant his-tagged hLamR purification. However, no matter how many parameters and condition that we tried, we still found difficulty to get rid of "the most common", around 100 kDa of unspecific protein out of Ni-NTA purification. Therefore, we applied the Ni-NTA purified protein to size exclusion chromatography (SEC) and harvested molecules within a particular range size in multiple fractions (Fig. 8E and F). Then each of the fraction was stained with anti-hLamR antibody and anti-his-tag antibody to detect the right fraction for recombinant his-tagged hLamR protein. In Fig. 8G, fractions 9 and 10 are the only two fractions could be detected by anti-hLamR antibody and anti-his-tag antibody, therefore, we combined these fractions as the final hLamR protein product.

Optimizing recombinant hLamR expression and extraction

Although the optimal condition for purification procedure was found, the product yield was measured below mg scale, which was only sufficient for a few times of downstream applications. In order to improve protein product yield and reduce batch-batch inconsistency, the optimization of protein expression and extraction were needed. HEK293-T has been known as the cell can be easily transfected, about 80% transfection efficiency has been reported (ref.) and it can have stronger transient expression over stable line expression sometimes (ref.). Furthermore, the effect by containing the selection marker, puromycin, in the medium on recombinant hLamR expression level has not yet been researched. Thus, the expression levels of recombinant hLamR were compared in HEK293T-Lenti transduced stable line (MOI 10) with and without

puromycin, HEK293-T transfected with 2μg and 4μg pLV-EF1α-6xHis-hLamR-IRES-Puro plasmid, and naïve HEK293-T. 24 hours after transfection, we changed the medium to puromycin-containing one for transfected cells and all the cells were harvested at 48 hours post-transfection. The western blotting revealed a 1.65-fold and a 2.02-fold hLamR expression in HEK293-T lenti-transduced stable line, without and with puromycin, respectively, compared to naïve cell. Interestingly, HEK293-T transfected with 2μg and 4μg plasmids exhibited 2-fold and 2.25-fold expression over naïve cells, respectively (Fig. 7A). Thus, we were able to know that containing puromycin in the medium have a benefit on recombinant hLamR yield. Although, the expression level between stable line and transient expression seems similar, a room for optimization, such as on plasmid amount transfected and harvest timepoint, was also observed in this initial screening. Most of transient expressions have highest target protein expression level at 48hr post-transfection or after (ref.). However, the pLV-EF1a-6xHIS-hLamR-IRES-Puro plasmid used in transfection contains a puromycin-resistance gene, so it might be worthwhile to screen multiple timepoints for best protein expression level by puromycin selection. Subsequently, the hLamR protein expression level in naïve cells, cells transfected with 5μg and 10μg of plasmids were compared. Cells were harvest at 24, 48, 72 and 96hr post-transfection. As the result, transfection with 10μg has superior hLamR expression than transfection with 5μg in each timepoint, 48hr was the highest as 3.66-fold higher than naïve control among all the groups (Fig. 7B). In fact, we also transfected pLV-EF1a-6xHIS-hLamR-IRES-Puro plasmid to Lenti-transduced HEK293-T cells to see if combined transient and stable expression induces higher recombinant hLamR expression level (Data was not shown). However, the expression of hLamR seemed to saturate and no significant differences on hLamR yield were found between transfection to HEK293-T lenti-transduced stable line and naïve cells. In additional to improve protein yield from expression aspect, we had performed an extraction buffer optimization study to solubilize more hLamR protein from the cells. In the first round of extraction buffer optimization, HEK 293T-lenti transduced cells were lysed by extraction buffer with different detergents or combinations including NP-40, TWEEN-20, digitonin, NP40/ TWEEN-20, NP-40/digitonin and TWEEN-20/digitonin. After lysis, the supernatant and pellet fraction of each group above were examined in western blotting to understand the best buffer for hLamR solubilization. In **Fig. 7C**, 2.28-fold, 2.59-fold, 2.72-fold and 2.6-fold of hLamR were detected in the supernatant fraction of TWEEN-20, digitonin, NP-40/digitonin and TWEEN-20/digitonin group, compared to the non-detergent control. In contrast, the pellet fraction of TWEEN-20, digitonin, NP-40/digitonin and TWEEN-20/digitonin group have lower hLamR protein level as 0.67-fold, 0.4-fold, 0.75-fold and 0.39-fold, respectively. The increases of hLamR protein level in supernatant and

decreases in the pellet, which suggests that the hLamR protein solubility was increased by the adding of detergents, especially TWEEN-20 and digitonin. Since these two detergents worked well alone or in accompanied with others, also, TWEEN-20 was already used for the washing steps in the purification process, 0.05% TWEEN-20 and 1% digitonin went into next round for comparing to 1% CHAPS. The same experiment was conducted again with different detergent groups including digitonin, CHAPS, digitonin/CHAPS, only this time his-tag was detected as well. The hLamR protein levels in supernatant fraction were 1.63-fold, 2.45-fold and 2.34-fold with the adding of digitonin, CHAPS and digitonin/CHAPS, respectively, by anti-hLamR blotting. A similar trend was found via his-tag blotting, the his-tagged protein levels were 1.27-fold, 1.97-fold and 2.05-fold in above groups, respectively. However, hLamR protein levels detected by anti-hLamR antibody were not significantly decreased in the pellet fraction and were even increased in his-tag blotting (Fig. 7D). Nonetheless, we were able to prove the benefit of having 1% CHAPS with 0.05% TWEEN-20 as the most appropriate detergents in the extraction buffer for recombinant hLamR's solubilization.

Discussions

Choosing peptide as a delivery agent for CNS therapeutics could bring a couples of benefits. Frist, the ease to be developed, engineered and manufactured. Peptides have a relatively small molecular weights, the whole sequences are generally within 30 amino acids and they can be synthesized by SPSS, whereas, for example, monoclonal antibodes have molecular weights of 150KDa, the development process is laborious and them needed to be produced by cell lines or animals. Second, the chemical diversity allows peptide to be conjugated with most of therapeutic molecules without causing steric hindrance.

Among the transporter/receptor mediated delivery, peptide-based methods usually have relatively low affinity. The dissociation constant of peptides is generally between nanomole to micromole level, whereas proteins and antibodies are between picomole to nanomole (ref). This property of peptide delivery comes with both advantage and disadvantage. The disadvantage is obvious, lower affinity leads to poorer bioavailability, when lesser amount of therapeutic distribute to the target site, the higher the dose is required, which caused certain degree of off-target and side effects. However, the lower affinity can bring advantage too. When the peptide-drug conjugates bind to the specific target receptor on the cell surface, the cell intake the whole ligand and receptor complex by the endocytosis, the peptide binder's low affinity increase the possibility for peptide-drug conjugate to dissociate from the receptor during cellular trafficking process and can be delivered to the final cellular therapeutic locations.

In this report, we suggested TAxI peptide is not only CNS targeting peptide, but only has potential to target delivery therapeutics to cancer cells. Although the affinity to HEK293-T, noncancer cell is weak, the binding was existing. Through further sequence modification and to identify specific environment for delivery, future study to decreasing the binding in non-cancer cell is warranted. Previous reports haven proved that hLamR could serve as a target for therapeutic approaches to treating cancer and Alzheimer's disease (Jovanoic et al., 2015). The flexibility of TAxI peptide for possible targeting two areas of disease is highly indulging.

TAxI peptide binds the cells through the interaction with hLamR on the cell surface. In other words, hLamR is the target receptor for TAxI delivery. Through sequence modification and multivalent polymerization, the affinity of TAxI peptide was demonstrated to be increased. Chondroitin Sulfate (CS) acted as a positive allosteric modulator for facilitating the association between TAxI and hLamR. Due to the high

expression of hLamR and CS in many types of cancer cell, TAxI-based delivery has potential to mobilize promising therapeutics to CNS and tumors.

References

Ahlschwede, K. M., Curran, G. L., Rosenberg, J. T., Grant, S. C., Sarkar, G., Jenkins, R. B., Ramakrishnan, S., Poduslo, J. F. and Kandimalla, K. K. (2019). Cationic carrier peptide enhances cerebrovascular targeting of nanoparticles in Alzheimer's disease brain. Nanomedicine 16:258-266.

Amano T, Fu L, Marshak A, Kwak O, Shi YB. Spatio-temporal regulation and cleavage by matrix metalloproteinase stromelysin-3 implicate a role for laminin receptor in intestinal remodeling during Xenopus laevis metamorphosis. Developmental Dynamics. 2005a; 234:190–200. [PubMed: 16059908]

Amano T, Kwak O, Fu L, Marshak A, Shi YB. The matrix metalloproteinase stromelysin-3 cleaves laminin receptor at two distinct sites between the transmembrane domain and laminin binding sequence within the extracellular domain. Cell Research. 2005b; 15:150–159. [PubMed: 15780176]

Ando K, Miyazaki Y, Sawayama Y, Tominaga S, Matsuo E, Yamasaki R, Inoue Y, Iwanaga M, Imanishi D, Tsushima H, Fukushima T, Imaizumi Y, Taguchi J, Yoshida S, Hata T, Tomonaga M. High expression of 67-kDa laminin receptor relates to the proliferation of leukemia cells and increases expression of GM-CSF receptor. Experimental Hematology. 2011; 39:179–186. e4. [PubMed: 21056082]

Anger, A. M., Armache, J. P., Berninghausen, O., Habeck, M., Subklewe, M., Wilson, D. N. and Beckmann, R. (2013). Structures of the human and Drosophila 80S ribosome. Nature 497:80–85.

Ardini, E., Pesole, G., Tagliabue, E., Magnifico, A., Castronovo, V., Sobel, M. E., Colnaghi, M. I. and Menard, S. (1998). The 67-kDa laminin receptor originated from a ribosomal protein that acquired a dual function during evolution. Mol Biol Evol. 15:1017–1025.

Ardini E, Sporchia B, Pollegioni L, Modugno M, Ghirelli C, Castiglioni F, Tagliabue E, Menard S. Identification of a novel function for 67-kDa laminin receptor: increase in laminin degradation rate and release of motility fragments. Cancer Research. 2002; 62:1321–1325. [PubMed: 11888899]

Ardini, E., Tagliabue, E., Magnifico, A., Buto, S., Castronovo, V., Colnaghi, M. I. and

Armstrong, M. J. and Okun, M. S. (2020). Diagnosis and Treatment of Parkinson Disease: A Review. JAMA 323(6):548-560.
Abbott, N. J. and Rönnbäck, L. and Hansson, E. (2006). Nat Rev Neurosci 7(1):41-53.

Atri, A. (2019). Current and future treatments in Alzheimer's disease. Semin Neurol 39:227-240.

Auth D, Brawerman G. A 33-kDa polypeptide with homology to the laminin receptor: component of translation machinery. Proceedings of the National Academy of Sciences of the United States of America. 1992; 89:4368–4372. [PubMed: 1374897]

Barchet, T. M. and Amiji, M. M. (2009). Challenges and opportunities in CNS delivery of therapeutics for neurodegenerative diseases. Expert Opin Drug Deliv 6(3): 211-25.

Basson CT, Knowles WJ, Bell L, Albelda SM, Castronovo V, Liotta LA, Madri JA. Spatiotemporal segregation of endothelial cell integrin and nonintegrin extracellular matrix-binding proteins during adhesion events. Journal of Cell Biology. 1990; 110:789–801. [PubMed: 2407741]

Ben-Shem A, Garreau de Loubresse N, Melnikov S, Jenner L, Yusupova G, Yusupov M. The structure of the eukaryotic ribosome at 3.0 A resolution. Science. 2011; 334:1524–1529. [PubMed: 22096102]

Bernard A, Gao-Li J, Franco CA, Bouceba T, Huet A, Li Z. Laminin receptor involvement in the anti-angiogenic activity of pigment epithelium-derived factor. Journal of Biological Chemistry. 2009; 284:10480–10490. [PubMed: 19224861]

Berno V, Porrini D, Castiglioni F, Campiglio M, Casalini P, Pupa SM, Balsari A, Menard S, Tagliabue E. The 67 kDa laminin receptor increases tumor aggressiveness by remodeling laminin-1. Endocrine Related Cancer. 2005; 12:393–406. [PubMed: 15947111]

Bloch, J., Bachoud-Lévi, A. C., Déglon, N., Lefaucheur, J. P., Winkel, L., Palfi, S., Nguyen, J. P., Bourdet, C., Gaura, V., Remy, P., Brugières, P., Boisse, M-F., Baudic, S., Cesaro, P., Hantraye, P., Aebischer, P. and Peschanski, M. (2004). Neuroprotective gene therapy for Huntington's disease, using polymer-encapsulated cells engineered to secrete human ciliary neurotrophic factor: results of a phase I study. Hum Gene Ther

15(10):968-75.

Brown, S. S., Malinoff, H. L. and Wicha, M. S. (1983). Connectin: cell surface protein that binds both laminin and actin. Proceedings of the National Academy of Sciences of the United States of America 80:5927–5930.

Burgess, A. and Hynynenm, K. (2013). Noninvasive and targeted drug delivery to the brain using focused ultrasound. ACS Chem Neurosci 17;4(4):519-26.
Buckner, R. L., Snyder, A. Z., Shannon, B. J., LaRossa, G., Sachs, R., Fotenos, A. F., Sheline, Y. I., Klunk, W. E., Mathis, C. A., Morris, J. C. and Mintun, M. A. (2005). Molecular, structural, and functional characterization of Alzheimer's disease: evidence for a relationship between default activity, amyloid, and memory. J Neurosci 25(34):7709-17.

Castronovo, V., Taraboletti, G. and Sobel, M. E. (1991). Functional domains of the 67-kDa laminin receptor precursor. J Biol Chem 266(30):20440-6.

Chen J, Carcamo JM, Borquez-Ojeda O, Erdjument-Bromage H, Tempst P, Golde DW. The laminin receptor modulates granulocyte-macrophage colony-stimulating factor receptor complex formation and modulates its signaling. Proceedings of the National Academy of Sciences of the United States of America. 2003; 100:14000–14005. [PubMed: 14614142]

Choudhury, S. R., Harris, A. F., Cabral, D. J., Keeler, A. M., Sapp, E., Ferreira, J. S., Gray-Edwards, H. L., Johnson, J. A., Johnson, A. K. Su, Q., Stoica, L., DiFiglia, M., Aronin, N. Martin, D. R., Gao, G. and Sena-Esteves, M. (2016). Widespread Central Nervous System Gene Transfer and Silencing After Systemic Delivery of Novel AAV-AS Vector. Mol Ther 24(4):726-35.

Chu, D. S. H., Schellinger, J. G., Bocek, M. J., Johnson, R. N. and Pun, S. H. (2013). Optimization of Tet1 Ligand Density in HPMA-Co-Oligolysine Copolymers for Targeted Neuronal Gene Delivery. Biomaterials 34(37):9632-7.

Davis CM, Papadopoulos V, Jia MC, Yamada Y, Kleinman HK, Dym M. Identification and partial characterization of laminin binding proteins in immature rat Sertoli cells. Experimental Cell Research. 1991; 193:262–273. [PubMed: 2004643]

Deuschl, G., Parmar, P., Brainin, M. and Murray, C. (2019). The global burden of

neurological disorders: translating evidence into policy. Lancet Neurol 19(3):255-265.

DiGiacomo, V. and Meruelo, D. (2016). Looking into laminin receptor: critical discussion regarding the non-integrin 37/67-kDa laminin receptor/RPSA protein. Biol Rev Camb Philos Soc 91(2):288-310.

Dong, X. (2018). Current Strategies for Brain Drug Delivery. Theranostics 8(6):1481-1493.

Dyck, S. M. and Karimi-Abdolrezaee, S. (2015). Chondroitin sulfate proteoglycans: Key modulators in the developing and pathologic central nervous system. Exp Neurol 269:169-87.

Fatehullah A, Doherty C, Pivato G, Allen G, Devine L, Nelson J, Timson DJ. Interactions of the 67 kDa laminin receptor and its precursor with laminin. Bioscience Reports. 2010; 30:73–79.

Federici, T. and Boulis, N. M. (2006). Gene-based treatment of motor neuron diseases. Muscle Nerve 33(3):302-23.

Federoff, H. J. (1999). Novel targets for CNS gene therapy. Gene Ther 6(12):1907-8.
Feigin, V. L., Vos, T., Nichols, E., Owolabi, M. O., Carroll, W. M., Dichgans, M., Huwyler, J., Wu, D. and Pardridge, W. M. (1996). Brain drug delivery of small molecules using immunoliposomes. Proc Natl Acad Sci U S A 93(24):14164-9.

Fichter, K. M., Zhang, L., Kiick, K. L., and Reineke, T. M. (2008). Peptide-functionalized poly(ethylene glycol) star polymers: DNA delivery vehicles with multivalent molecular architecture. Bioconjug Chem 19(1):76-88.

Formisano P, Ragno P, Pesapane A, Alfano D, Alberobello AT, Rea VE, Giusto R, Rossi FW, Beguinot F, Rossi G, Montuori N. PED/PEA-15 interacts with the 67 kD laminin receptor and regulates cell adhesion, migration, proliferation and apoptosis. Journal of Cellular and Molecular Medicine. 2012; 16:1435–1446. [PubMed: 21895963]

Fujimura, Y., Yamada, k and Tachibana, H. (2005). A lipid raft-associated 67kDa laminin receptor mediates suppressive effect of epigallocatechin-3-O-gallate on FcepsilonRI expression. Biochem Biophys Res Commun 336(2):674-81.

GBD 2016 Neurology Collaborators (2019). Global, regional, and national burden of neurological disorders, 1990-2016: a systematic analysis for the Global Burden of Disease Study 2016. Lancet Neurol 18(5):459-480.

Givant-Horwitz V, Davidson B, Reich R. Laminin-induced signaling in tumor cells: the role of the M(r) 67,000 laminin receptor. Cancer Research. 2004; 64:3572–3579. [PubMed: 15150114]

Gray, S. J., Kalburgi, S. N., McCown, T. J., Samulski, R. J. (2013). Global CNS gene delivery and evasion of anti-AAV-neutralizing antibodies by intrathecal AAV administration in non-human primates. Gene Ther 20(4):450-9.

Guerra-Rebollo M, Mateo F, Franke K, Huen MS, Lopitz-Otsoa F, Rodriguez MS, Plans V, Thomson TM. Nucleolar exit of RNF8 and BRCA1 in response to DNA damage. Experimental Cell Research. 2012; 318:2365–2376. [PubMed: 22814251]

Guirguis R, Margulies I, Taraboletti G, Schiffmann E, Liotta L. Cytokine-induced pseudopodial protrusion is coupled to tumour cell migration. Nature. 1987; 329:261–263. [PubMed: 2957596]

Guo, N. H., Krutzsch, H. C., Vogel, T. and Roberts, D. D. (1992). Interactions of a laminin-binding peptide from a 33-kDa protein related to the 67-kDa laminin receptor with laminin and melanoma cells are heparin-dependent. J Biol Chem ;267(25):17743-7.

Howard, R., McShane, R., Lindesay, J, Ritchie, C., Baldwin, A., Barber, R., Burns, A., Dening, T., Findlay, D., Holmes, C., Jones, R., Jones, R., McKeith, I., Macharouthu, A., O'Brien, J., Sheehan, B., Juszczak, E., Katona, C., Hills, R., Knapp, M., Ballard, C., Brown, R. G., Banerjee, S., Adams, J., Johnson, T., Bentham, P. and Phillips, P. P. J.. Nursing home placement in the donepezil and memantine in moderate to severe Alzheimer's disease (DOMINO-AD) trial: secondary and post-hoc analyses. *Lancet Neurol* 14(12):1171-1181.

Jamieson KV, Wu J, Hubbard SR, Meruelo D. Crystal structure of the human laminin receptor precursor. Journal of Biological Chemistry. 2008; 283:3002–3005. [PubMed: 18063583]

Johnson, R. N., Chu, D. S. H., Shi, J., Schellinger, J. G., Carlson, P. M. and Pun, S. H. (2011) HPMA-oligolysine copolymers for gene delivery: optimization of peptide length and polymer molecular weight. J Control Release 155(2):303-11.

Jeong, W., Bu, J., Kubiatowicz, L. J., Chen, S. S., Kim, Y. and Hong, S. (2018). Peptide-nanoparticle conjugates: a next generation of diagnostic and therapeutic platforms? Nano Converg ;5(1):38.

Jovanovic, K., Chetty, C. J., Khumalo, T., Dias, B. D. C., Ferreira, E., Malindisa, S. T., Caveney, R., Letsolo, B. T. and Weiss, S. F. T. Novel patented therapeutic approaches targeting the 37/67 kDa laminin receptor for treatment of cancer and Alzheimer's disease. Expert Opin Ther Pat 2015 May;25(5):567-82.

Kageyama, T., Nakamura, M., Matsuo, A., Yamasaki, Y., Takakura, Y., Hashida, M., Kanai, Y., Naito, M., Tsuruo, T., Minato, N. and Shimohama, S. (2000) The 4F2hc/LAT1 complex transports L-DOPA across the blood-brain barrier. Brain Res 6;879(1-2):115-21.

Kanyo, N., Kovacs, K. D., Saftics, A., Szekacs, I., Peter, B., Santa-Maria, A. R., Walter, F. R., Dér, A., Deli, M. A. and Horvath, R. (2020). Glycocalyx regulates the strength and kinetics of cancer cell adhesion revealed by biophysical models based on high resolution label-free optical data. Sci Rep 10(1):22422.

Karpatova M, Tagliabue E, Castronovo V, Magnifico A, Ardini E, Morelli D, Belotti D, Colnaghi MI, Menard S. Shedding of the 67-kD laminin receptor by human cancer cells. Journal of Cellular Biochemistry. 1996; 60:226–234. [PubMed: 8655633]

Kazmin, D. A., Hoyt, T. R., Taubner, L., Teintze, M. and Starkey, J. R. (2000). J Mol Biol 298(3):431-45.

Keppel E, Schaller HC. A 33 kDa protein with sequence homology to the 'laminin binding protein' is associated with the cytoskeleton in hydra and in mammalian cells. Journal of Cell Science. 1991; 100(Pt 4):789–797. [PubMed: 1726100]

Kim KJ, Chung JW, Kim KS. 67-kDa laminin receptor promotes internalization of cytotoxic necrotizing factor 1-expressing Escherichia coli K1 into human brain microvascular endothelial cells. Journal of Biological Chemistry. 2005; 280:1360–1368. [PubMed: 15516338]

Kinoshita K, Kaneda Y, Sato M, Saeki Y, Wataya-Kaneda M, Hoffmann A. LBP-p40 binds DNA tightly through associations with histones H2A, H2B, and H4. Biochemical and Biophysical Research Communications. 1998; 253:277–282. [PubMed: 9878528]

Ku HC, Chang HH, Liu HC, Hsiao CH, Lee MJ, Hu YJ, Hung PF, Liu CW, Kao YH. Green tea (−)-epigallocatechin gallate inhibits insulin stimulation of 3T3-L1 preadipocyte mitogenesis via the 67-kDa laminin receptor pathway. American Journal of Physiology: Cell Physiology. 2009; 297:C121–C132. [PubMed: 19176763]

Ku HC, Liu HS, Hung PF, Chen CL, Liu HC, Chang HH, Tsuei YW, Shih LJ, Lin CL, Lin CM, Kao YH. Green tea (−)-epigallocatechin gallate inhibits IGF-I and IGF-II stimulation of 3T3-L1 preadipocyte mitogenesis via the 67-kDa laminin receptor, but not AMP-activated protein kinase pathway. Molecular Nutrition & Food Research. 2012; 56:580–592. [PubMed: 22495985]

Kumazoe, M., Sugihara, K., Tsukamoto, S., Huang, Y., Tsurudome, Y., Suzuki, T., Suemasu, Y., Ueda, N., Yamashita, S., Kim, Y., Yamada, K. and Tachibana1, H. (2013). 67-kDa laminin receptor increases cGMP to induce cancer-selective apoptosis. J Clin Invest 123(2): 787–799.

Landowski TH, Dratz EA, Starkey JR. Studies of the structure of the metastasis-associated 67 kDa laminin binding protein: fatty acid acylation and evidence supporting dimerization of the 32 kDa gene product to form the mature protein. Biochemistry. 1995a; 34:11276–11287. [PubMed: 7669786]

Lin, C. and Anseth, K. S. (2009). Controlling Affinity Binding with Peptide-Functionalized Poly(ethylene glycol) Hydrogels. Adv Funct Mater 19(14):2325.

Lockman, P. R., Oyewumi, M. O., Koziara, J. M., Roder, K. E., Mumper, R. J. and Allen, D. D. (2003) Brain uptake of thiamine-coated nanoparticles. J Control Release 12;93(3):271-82.

Malinoff HL, Wicha MS. Isolation of a cell surface receptor protein for laminin from murine fibrosarcoma cells. Journal of Cell Biology. 1983; 96:1475–1479. [PubMed: 6302102]

Malygin AA, Babaylova ES, Loktev VB, Karpova GG. A region in the C-terminal

domain of ribosomal protein SA required for binding of SA to the human 40S ribosomal subunit. Biochimie. 2011; 93:612–617. [PubMed: 21167900]

Maroto, M., Fernández-Morales, J., Padín, J. F., González, J. C., Hernández-Guijo, J. M., Montell, E., Vergés, J., de Diego, A. M. G. and García, A. G. (2013). Chondroitin sulfate, a major component of the perineuronal net, elicits inward currents, cell depolarization, and calcium transients by acting on AMPA and kainate receptors of hippocampal neurons. J Neurochem 125(2):205-13.

Menard, S. (1997). Co-regulation and physical association of the 67-kDa monomeric laminin receptor and the alpha6beta4 integrin. J Biol Chem. 272:2342–2345.

Minn, A., Ghersi-Egea J. F., Perrin, R., Leininger, B. and Siest, G. (1991). Drug metabolizing enzymes in the brain and cerebral microvessels. Brain Res Brain Res Rev 16(1):65-82.

Moss BL, Taubner L, Sample YK, Kazmin DA, Copie V, Starkey JR. Tumor shedding of laminin binding protein modulates angiostatin production in vitro and interferes with plasmin-derived inhibition of angiogenesis in aortic ring cultures. International Journal of Cancer. 2006; 118:2421–2432. [PubMed: 16380995]

Nagahara, H., Vocero-Akbani, A. M., Snyder, E. L., Ho, A., Latham, D. G., Lissy, N. A., Becker-Hapak, M., Ezhevsky, S. A. and Dowdy, S. F. (1998). Transduction of full-length TAT fusion proteins into mammalian cells: TAT-p27Kip1 induces cell migration. Nat Med 4(12):1449-52.

Ngambenjawong, C. and Pun, S. H. (2017). Multivalent polymers displaying M2 macrophage-targeting peptides improve target binding avidity and serum stability. ACS Biomater Sci Eng ;3(9):2050-2053.

O'Donohue, M., Choesmel, V., Faubladier, M., Fichant, G. and Gleizes, P. (2010). Functional dichotomy of ribosomal proteins during the synthesis of mammalian 40S ribosomal subunits. J Cell Biol 190(5):853-66.

Pardridge, W. M. (1992). Recent developments in peptide drug delivery to the brain. Pharmacol Toxicol 71(1):3-10.

Pardridge, W. M. (2002). Drug and gene delivery to the brain: the vascular route.

Neuron 36(4):555-8.

Pardridge, W. M. (2005). The blood-brain barrier: bottleneck in brain drug development. NeuroRx 2(1):3-14.

Park E, Choi Y, Ahn E, Park I, Yun Y. The adaptor protein LAD/TSAd mediates laminin-dependent T cell migration via association with the 67 kDa laminin binding protein. Experimental and Molecular Medicine. 2009; 41:728–736. [PubMed: 19561400]

Pellegrini R, Martignone S, Menard S, Colnaghi MI. Laminin receptor expression and function in small-cell lung carcinoma. International Journal of Cancer. Supplement. 1994; 8:116–120.

Pesapane, A., Giovanni, C. D., Rossi, F. W., Alfano, D. Formisano, L. Ragno, P., Selleri, C., Montuori, N. and Lavecchia, A. (2015), Discovery of new small molecules inhibiting 67 kDa laminin receptor interaction with laminin and cancer cell invasion. Oncotarget 6(20):18116-33

Pringsheim, T., Wiltshire, K., Day, L., Dykeman, J., Steeves, T. and Jette, N. (2012). The incidence and prevalence of Huntington's disease: a systematic review and meta-analysis. Mov Disord 27(9):1083-91.

Rabl J, Leibundgut M, Ataide SF, Haag A, Ban N. Crystal structure of the eukaryotic 40S ribosomal subunit in complex with initiation factor 1. Science. 2011; 331:730–736. [PubMed: 21205638]

Radford, D. C., Yang, J., Doan, M. C., Li, L., Dixon, A. S., Owen, S. C. and Kopeček, J. (2020). Multivalent HER2-binding polymer conjugates facilitate rapid endocytosis and enhance intracellular drug delivery. J Control Release 319:285-299.

Rao NC, Barsky SH, Terranova VP, Liotta LA. Isolation of a tumor cell laminin receptor. Biochemical and Biophysical Research Communications. 1983; 111:804–808. [PubMed: 6301485]

Reese, T. S. and Karnovsky, M. J. (1967). J Cell Biol 34(1):207-17.

Rossi, A., Berger, K., Chen, H., Leslie, D., Mailman, R. B., Huang X (2018). Projection

of the prevalence of Parkinson's disease in the coming decades: Revisited. Mov Disord 33(1):156-159.

Rush J, Moritz A, Lee KA, Guo A, Goss VL, Spek EJ, Zhang H, Zha XM, Polakiewicz RD, Comb MJ. Immunoaffinity profiling of tyrosine phosphorylation in cancer cells. Nature Biotechnology. 2005; 23:94–101.

Salama RH, Muramatsu H, Zou K, Inui T, Kimura T, Muramatsu T. Midkine binds to 37-kDa laminin binding protein precursor, leading to nuclear transport of the complex. Experimental Cell Research. 2001; 270:13–20. [PubMed: 11597123]

Scheltens, P., Blennow, K. and Breteler, M. M. B, de Strooper, B., Frisoni, G. B., Salloway, S. and Van der Flier, W. M. Alzheimer's disease. Lancet 388(10043):505-517.

Scheiman J, Jamieson KV, Ziello J, Tseng JC, Meruelo D. Extraribosomal functions associated with the C terminus of the 37/67 kDa laminin receptor are required for maintaining cell viability. Cell Death & Disease. 2010a; 1:e42. [PubMed: 21243100]

Scheiman J, Tseng JC, Zheng Y, Meruelo D. Multiple functions of the 37/67-kd laminin receptor make it a suitable target for novel cancer gene therapy. Molecular Therapy. 2010b; 18:63–74. [PubMed: 19724263]

Shi, J., Schellinger, J. G. and Pun, S. H. (2013). Engineering biodegradable and multifunctional peptide-based polymers for gene delivery. J Biol Eng 7(1):25.
Taylor, J. P., Hardy, J. and Fischbeck, K. H. (2002). Science 296(5575):1991-5.

Soeda S, Ishida S, Honda O, Shimeno H, Nagamatsu A. Aminated fucoidan promotes the invasion of 3 LL cells through reconstituted basement membrane: its possible mechanism of action. Cancer Letters. 1994; 85:133–138. [PubMed: 7923097]

Sun, W., Xie, C., Wang, H. and Hu, Y. (2004). Specific role of polysorbate 80 coating on the targeting of nanoparticles to the brain. Biomaterials 25(15):3065-71.
Spencer, B. J and Verma, I. M. (2007). Targeted delivery of proteins across the blood-brain barrier. Proc Natl Acad Sci U S A 104(18):7594-9.

Tysnes, O. and Storstein, A. (2017). Epidemiology of Parkinson's disease. J Neural Transm (Vienna) 124(8):901-905.

Tsuji, A. and Tamai, I. (1999). Carrier-mediated or specialized transport of drugs across the blood-brain barrier. Adv Drug Deliv Rev 5;36(2-3):277-290.

Turpeenniemi-Hujanen T, Thorgeirsson UP, Rao CN, Liotta LA. Laminin increases the release of type IV collagenase from malignant cells. Journal of Biological Chemistry. 1986; 261:1883–1889. [PubMed: 3003087]

Umbaugh, C. S., Diaz-Quiñones, A., Neto, M. F., Shearer, J. J. and Figueiredo, M. L. (2017). A dock derived compound against laminin receptor (37 LR) exhibits anti-cancer properties in a prostate cancer cell line model. Oncotarget 9(5):5958-5978.

Vega, I. E., Cabrera, L. Y., Wygant, C. M., Velez-Ortiz, D and Counts, S. E. (2017). Alzheimer's Disease in the Latino Community: Intersection of Genetics and Social Determinants of Health. J Alzheimers Dis 58(4):979-992.

Venticinque L, Jamieson KV, Meruelo D. Interactions between laminin receptor and the cytoskeleton during translation and cell motility. PLoS One. 2011; 6:e15895. [PubMed: 21249134]

Venticinque L, Meruelo D. Comprehensive proteomic analysis of nonintegrin laminin receptor interacting proteins. Journal of Proteome Research. 2012; 11:4863–4872. [PubMed: 22909348]

Warren, K. E. (2018). Beyond the Blood:Brain Barrier: The Importance of Central Nervous System (CNS) Pharmacokinetics for the Treatment of CNS Tumors, Including Diffuse Intrinsic Pontine Glioma. Front Oncol 8:239.

Weeks BS, DiSalvo J, Kleinman HK. Laminin-mediated process formation in neuronal cells involves protein dephosphorylation. Journal of Neuroscience Research. 1990; 27:418–426. [PubMed: 1965840]

Weintraub, D., Comella, C. L. and Horn, S. (2008). Parkinson's disease--Part 1: Pathophysiology, symptoms, burden, diagnosis, and assessment. Am J Manag Care 14(2 Suppl):S40-48.

Weintraub, D., Comella, C. L. and Horn, S. (2008). Parkinson's disease – Part 2: Treatment of motor symptoms. Am J Manag Care 14(2 Suppl):S49-58.

Wu, L. P., Ahmadvand, D., Su, J., Hall, A., Tan, X., Farhangrazi, Z. S. and Moghimi, S. M. (2019). Crossing the blood-brain-barrier with nanoligand drug carriers self-assembled from a phage display peptide. Nat Commun 10(1):4635.

Yannariello-Brown J, Wewer U, Liotta L, Madri JA. Distribution of a 69-kD laminin-binding protein in aortic and microvascular endothelial cells: modulation during cell attachment, spreading, and migration. Journal of Cell Biology. 1988; 106:1773–1786. [PubMed: 2967300]

Yiannopoulou, K. G. and Papageorgiou, S. G. (2013). Current and future treatments for Alzheimer's disease. Ther Adv Neurol Disord 6:19-33.

Yu, Y. J., Zhang, Y., Kenrick, M., Hoyte, K. Luk, W. Lu, Y. Atwal, J., Elliott, J. M., Prabhu, S., Watts, R. J. and Dennis, M. S. (2011) Boosting brain uptake of a therapeutic antibody by reducing its affinity for a transcytosis target. Sci Transl Med 3(84):84ra44.

Zhou, Q. H., Boado, R. J., Hui, E. K., Lu, J. Z. and Pardridge, W. M. (2011). Chronic dosing of mice with a transferrin receptor monoclonal antibody-glial-derived neurotrophic factor fusion protein. Drug Metab Dispos 39(7):1149-54.

Zidane N, Ould-Abeih MB, Petit-Topin I, Bedouelle H. The folded and disordered domains of human ribosomal protein SA have both idiosyncratic and shared functions as membrane receptors. Bioscience Reports. 2013; 33:113–124.

Zlokovic, B. V. (2008). The blood-brain barrier in health and chronic neurodegenerative disorders. Neuron 57(2):178-201.

Zünkeler, B., Carson, R. E., Olson, J., Blasberg, R. G., DeVroom, H., Lutz, R. J., Saris, S. C., Wright, D. C., Kammerer, W., Patronas, N. J. Dedrick, R. L., Herscovitch, P. and Oldfield, E. H. (1996). Quantification and pharmacokinetics of blood-brain barrier disruption in humans. J Neurosurg 85(6):1056-65.

Figures

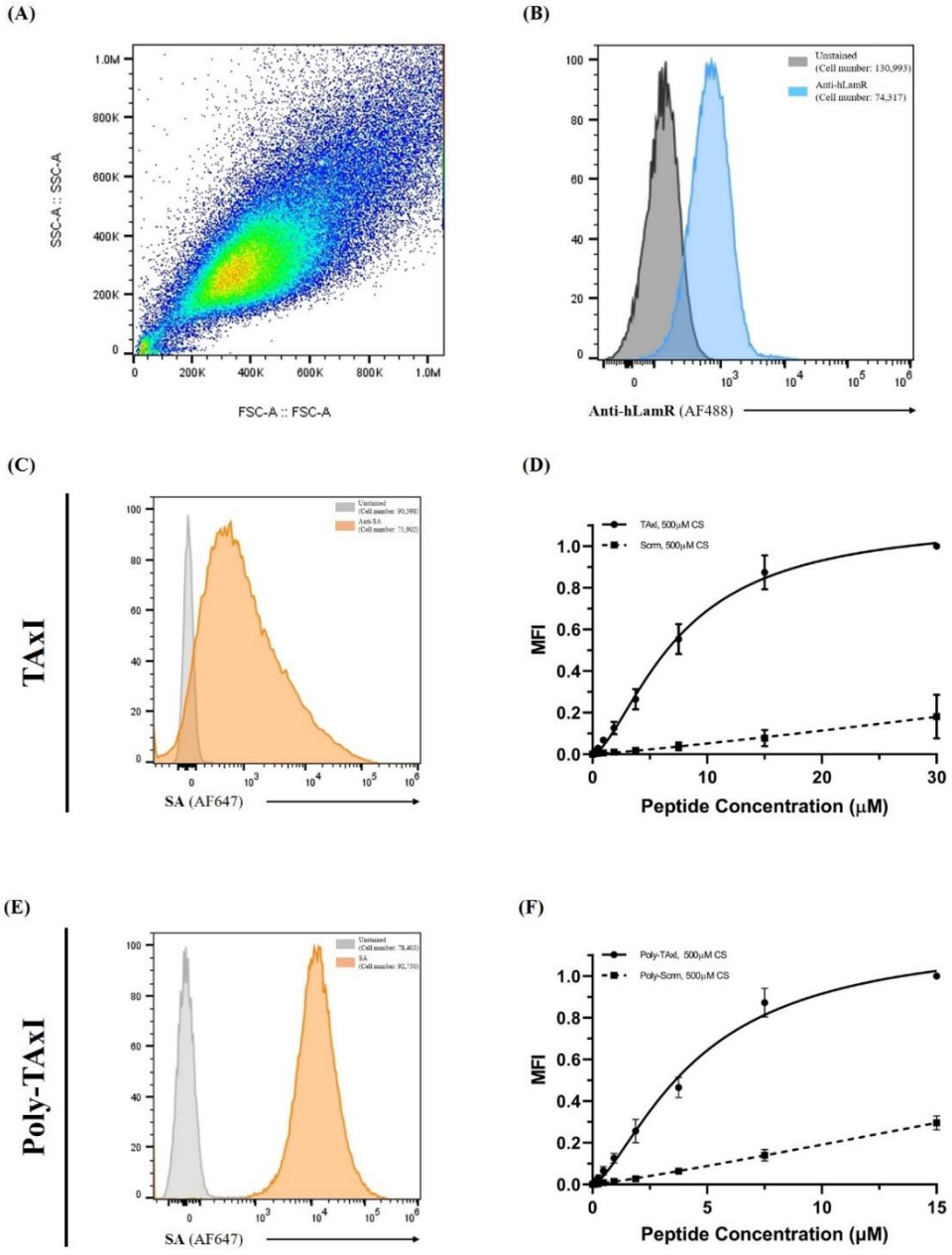

Figure 1. TAxI and Poly-TAxI Binding in HeLa Cells. (A) Pseudocolor plot view of HeLa cells collected by flow cytometry. **(B)** Histogram of hLamR staining in HeLa cells. Cells were labelled with anti-hLamR antibody and anti-mouse AF-488, or the latter only. **(C)** Histogram of TAxI peptide staining in HeLa cells. Cells were labelled with 30µg of biotinylated-TAxI and streptavidin (SA)-AF488, or the latter only. **(D)** TAxI and SCRM binding curves in HeLa cells. Cells were labelled with serial diluted of either biotinylated-TAxI or biotinylated-SCRM peptides with 500µM of chondroitin sulfate (CS) then stained with SA-AF488. **(E)** Histogram of TAxI peptide staining in HeLa cells. Cells were labelled with 15µg of biotinylated-Poly-TAxI and SA-AF488, or the latter only. **(F)** Poly-TAxI and Poly-SCRM binding curves in HeLa cells. Cells were labelled with serial diluted of either biotinylated-Poly-TAxI or biotinylated-Poly-SCRM peptides with 500µM of CS then stained with SA-AF488.

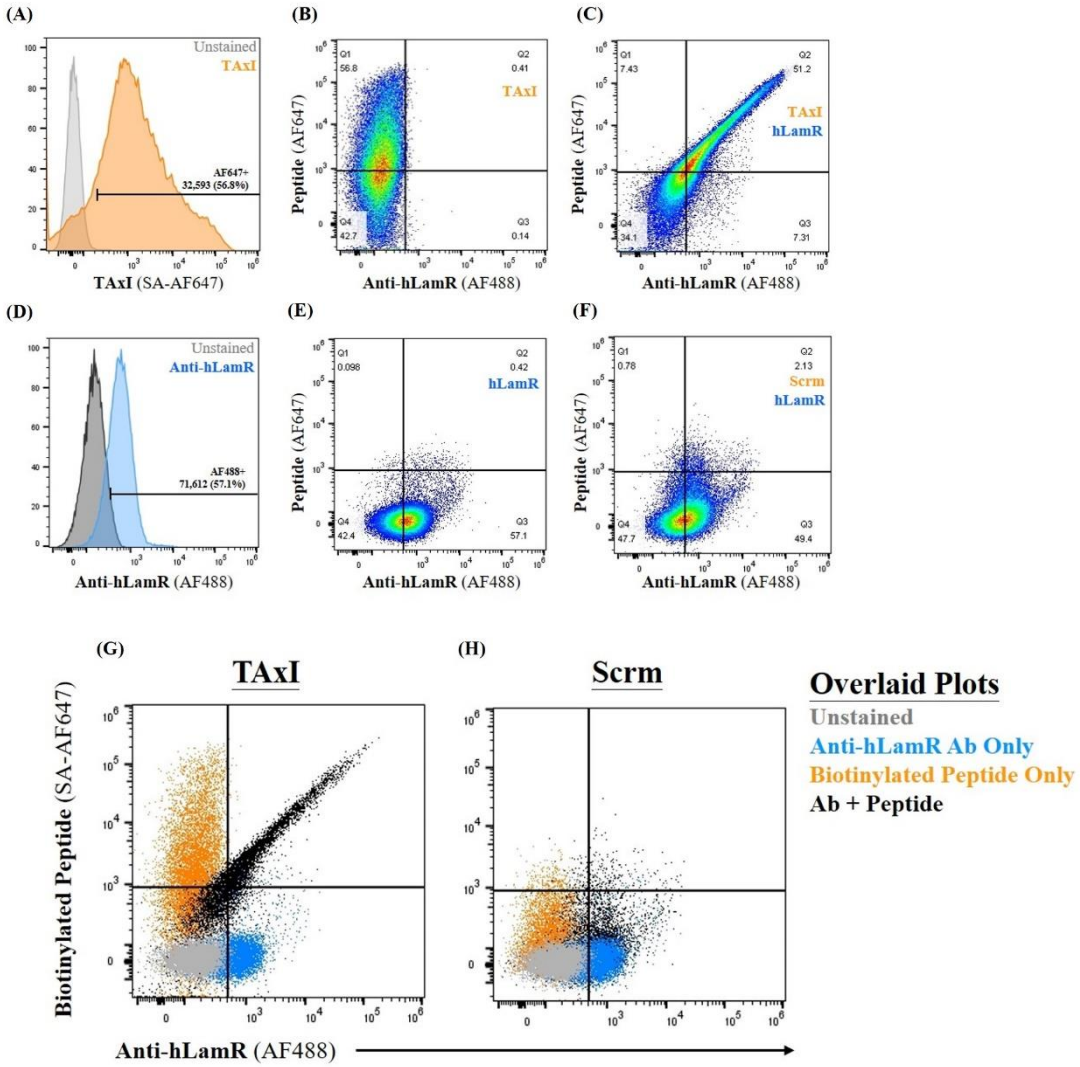

Figure 2. TAxI binds to cells via Laminin Receptor. (A) Histogram of TAxI peptide staining in HeLa cells. Cells were labelled with 30µg of biotinylated-TAxI and streptavidin (SA)-AF488, or the latter only. **(B)** Quadrant plot of cells labelled with 30µg TAxI, 56.8% of cells are AF-647 positive in quadrant 1. **(C)** Quadrant plot of cells co-labelled with 30µg TAxI and 1:100 anti-hLamR antibody, 51.2% of cells are AF-647 and AF-488 double positive in quadrant 2. **(D)** Histogram of hLamR staining in HeLa cells. Cells were labelled with anti-hLamR antibody and anti-mouse AF-488, or the latter only. **(E)** Quadrant plot of cells labelled with 1:100 anti-hLamR antibody, 57.1% of cells are AF-488 positive in quadrant 3. **(F)** Quadrant plot of cells co-labelled with 30µg SCRM and 1:100 anti-hLamR antibody, only 2.1% of cells are AF-647 and AF-488 double positive in quadrant 2. **(G)** Overlaid plot for TAxI and hLamR co-staining. **(H)** Overlaid plot for SCRM and hLamR co-staining.

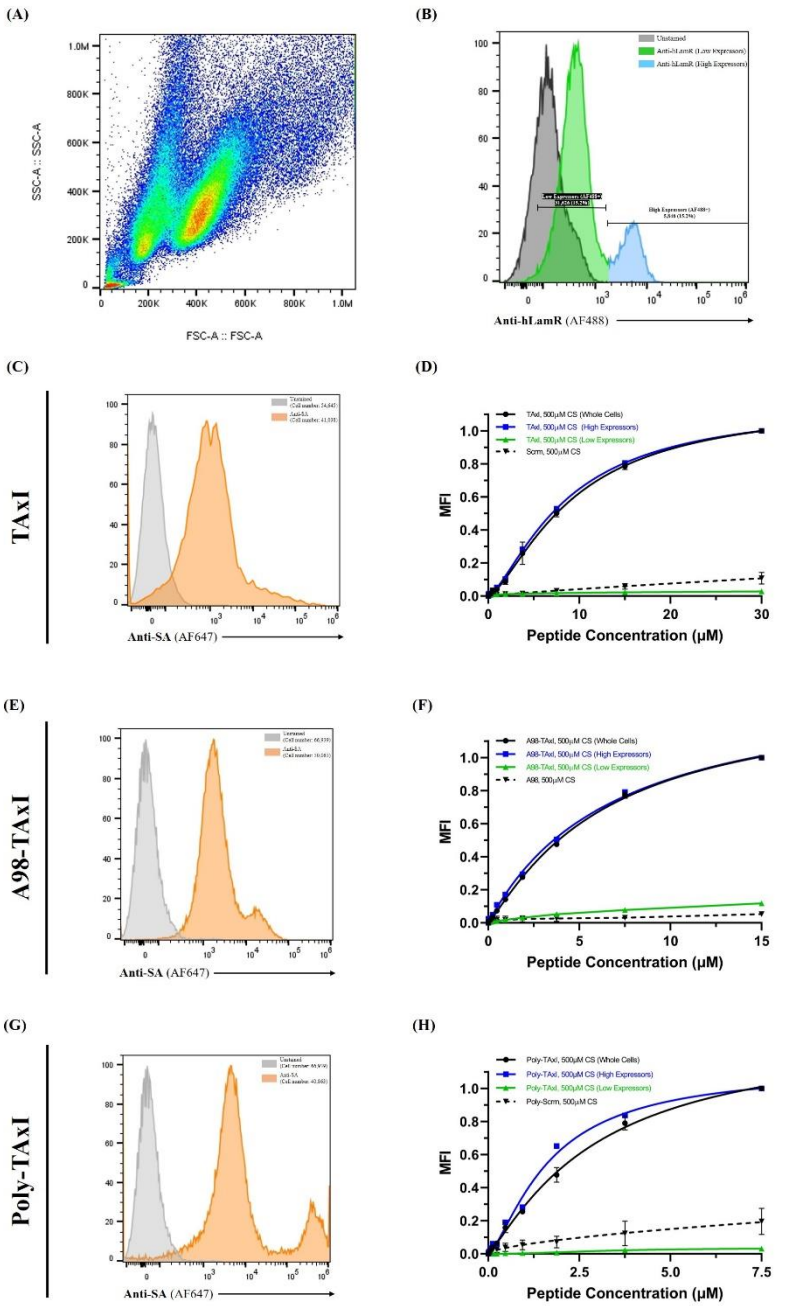

Figure 3. TAxI, A98-TAxI and Poly-TAxI Binding in GBM8 Cells. (A) Pseudocolor plot view of GBM8 cells collected by flow cytometry. **(B)** Histogram of hLamR staining in GBM8 cells. Cells were labelled with anti-hLamR antibody and anti-mouse AF-488, or the latter only. The low and high hLamR expressing cells were shown as green and blue peaks, respectively. **(C)** Histogram of TAxI peptide staining in GBM8 cells. Cells were labelled with 30μg of biotinylated-TAxI and streptavidin (SA)-AF488, or the latter only. **(D)** TAxI and SCRM binding curves in HeLa cells. Cells were labelled with serial diluted of either biotinylated-TAxI or biotinylated-SCRM peptides with 500μM CS then stained with SA-AF488. Blue lines are the binding curves for high expressors, whereas green lines are for low expressors. **(E)** Histogram of A98-TAxI peptide staining in GBM8 cells. Cells were labelled with 15μg of biotinylated-A98-TAxI and SA-AF488, or the latter only. **(F)** A98-TAxI and A98-SCRM binding curves in GBM8 cells. Cells were labelled with serial diluted of either biotinylated-A98-TAxI or biotinylated-A98-SCRM peptides with 500μM of CS then stained with SA-AF488. Blue lines are the binding curves for high expressors, whereas green lines are for low expressors. **(G)** Histogram of Poly-TAxI peptide staining in GBM8 cells. Cells were labelled with 7.5μg of biotinylated-Poly-TAxI and SA-AF488, or the latter only. **(H)** Poly-TAxI and Poly-SCRM binding curves in GBM8 cells. Cells were labelled with serial diluted of either biotinylated-Poly-TAxI or biotinylated-Poly-SCRM peptides with 500μM of CS then stained with SA-AF488. Blue lines are the binding curves for high expressors, whereas green lines are for low expressors.

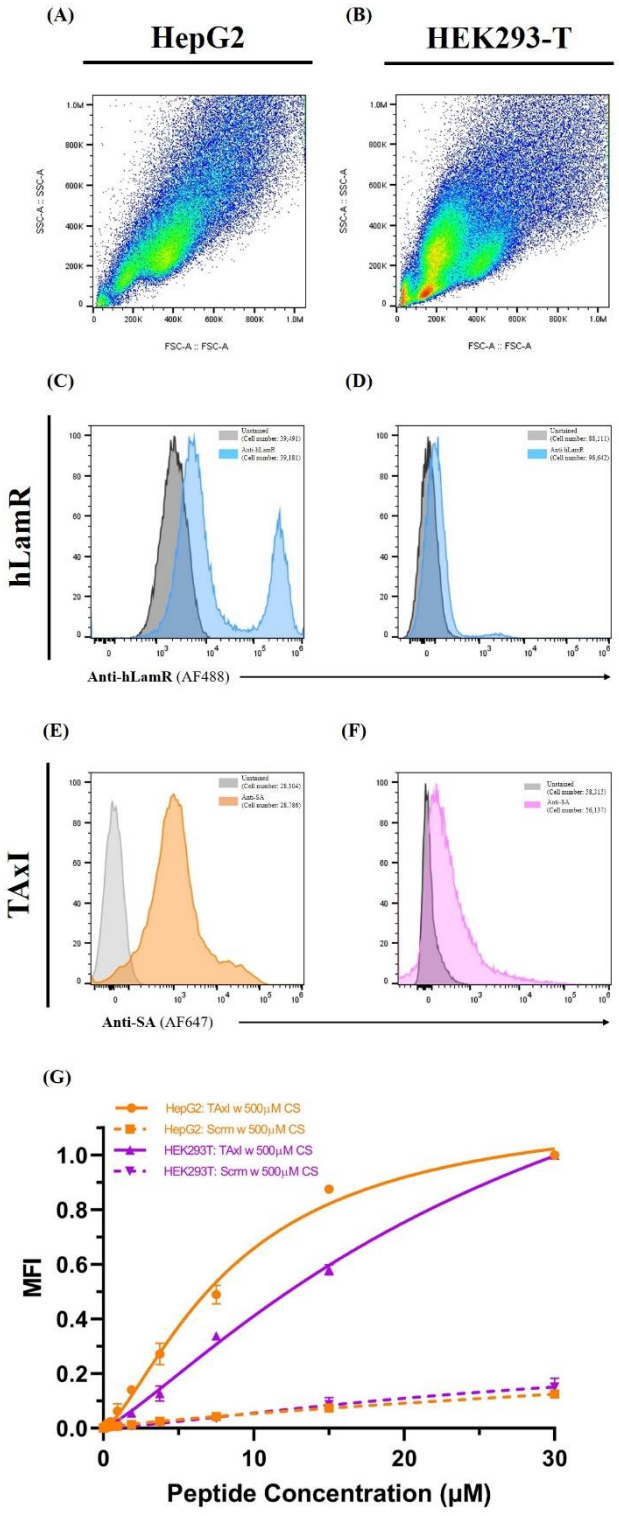

Figure 4. TAxI Demonstrates Prominent Binding to Cancer Cells than Non-cancer Cells. **(A)(B)** Pseudocolor plot view of HepG2 and HEK293-T cells collected by flow cytometry, respectively. **(C)(D)** Histogram of hLamR staining in HepG2 and HEK293-T cells, respectively. Cells were labelled with anti-hLamR antibody and anti-mouse AF-488, or the latter only. **(E)(F)** Histogram of TAxI peptide staining in HepG2 and HEK293-T cells, respectively. Cells were labelled with 30μg of biotinylated-TAxI and streptavidin (SA)-AF488, or the latter only. **(G)** TAxI and SCRM binding curves in HepG2 and HEK293-T cells, respectively. Cells were labelled with serial diluted of either biotinylated-TAxI or biotinylated-SCRM peptides with 500μM CS then stained with SA-AF488. Orange lines are the binding curves for HepG2, whereas purple lines are for HEK293-T.

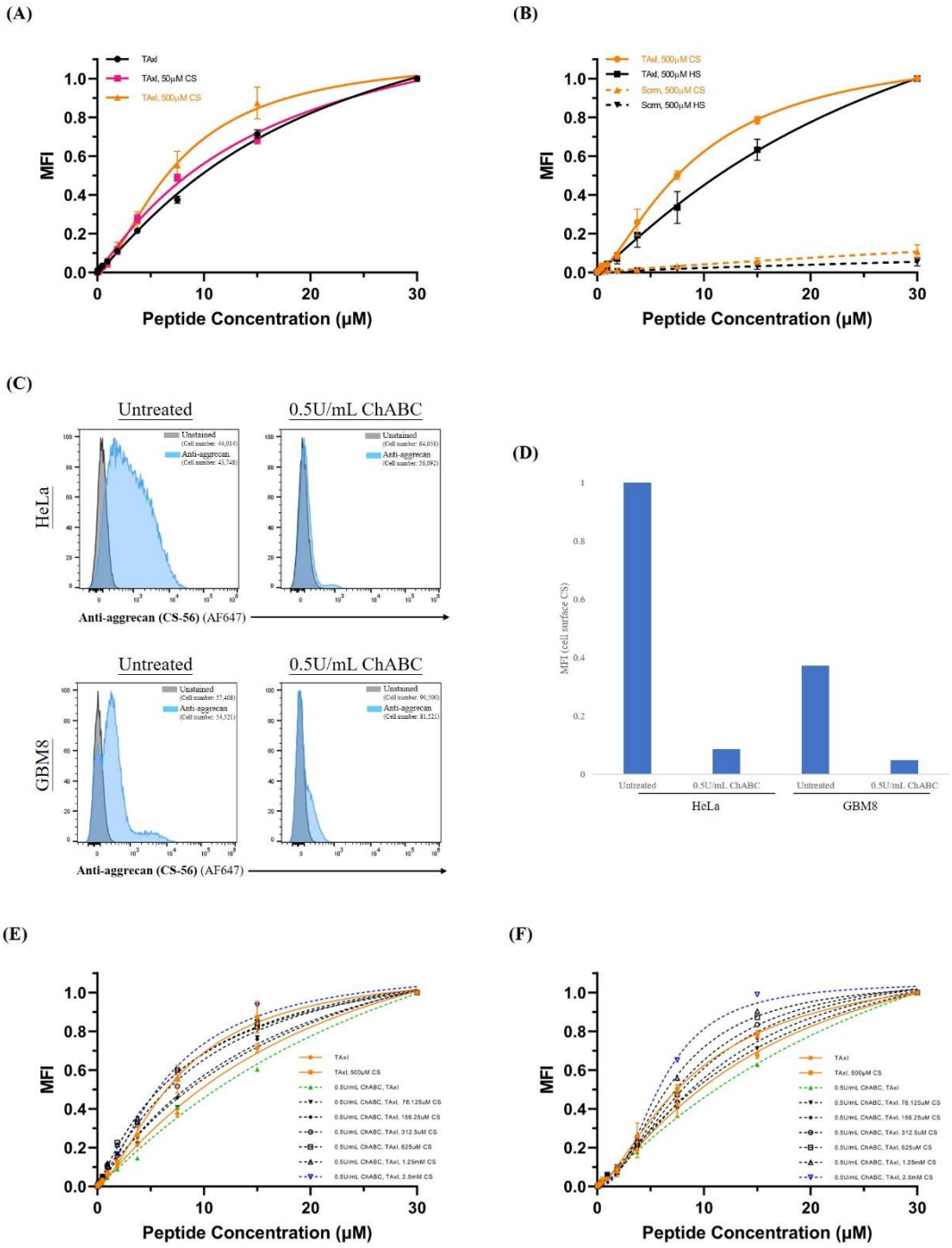

Figure 5. Chondroitin Sulfate (CS) facilitates the interaction between TAxI and hLamR. **(A)** CS helps TAxI's saturation to HeLa cells. HeLa cells were incubated with serial diluted biotinylated-TAxI peptides with 0, 50 and 500μM of CS, then stained with SA-AF647. **(B)** CS, but not heparan sulfate (HS), increases TAxI's affinity to cells. HeLa cells were incubated with serial diluted biotinylated-TAxI peptides with 500μM of CS or HS, then stained with SA-AF647. **(C)** Histogram of aggrecan (CS-56) staining of untreated and chondroitinase ABC (ChABC)-treated HeLa and HepG2 cells. Cells were either treated with 0.5U/mL ChABC or HBSS, then labelled with anti-aggrecan (CS-56) antibody and anti-mouse AF-647. **(D)** Surface CS level in untreated and ChABC-treated cells. (E)(F) CS rescues the affinity loss of TAxI in ChABC-treated HeLa and GBM8 cells. Different amount of soluble CS were co-supplemented with TAxI peptide to the ChABC-treated cells.

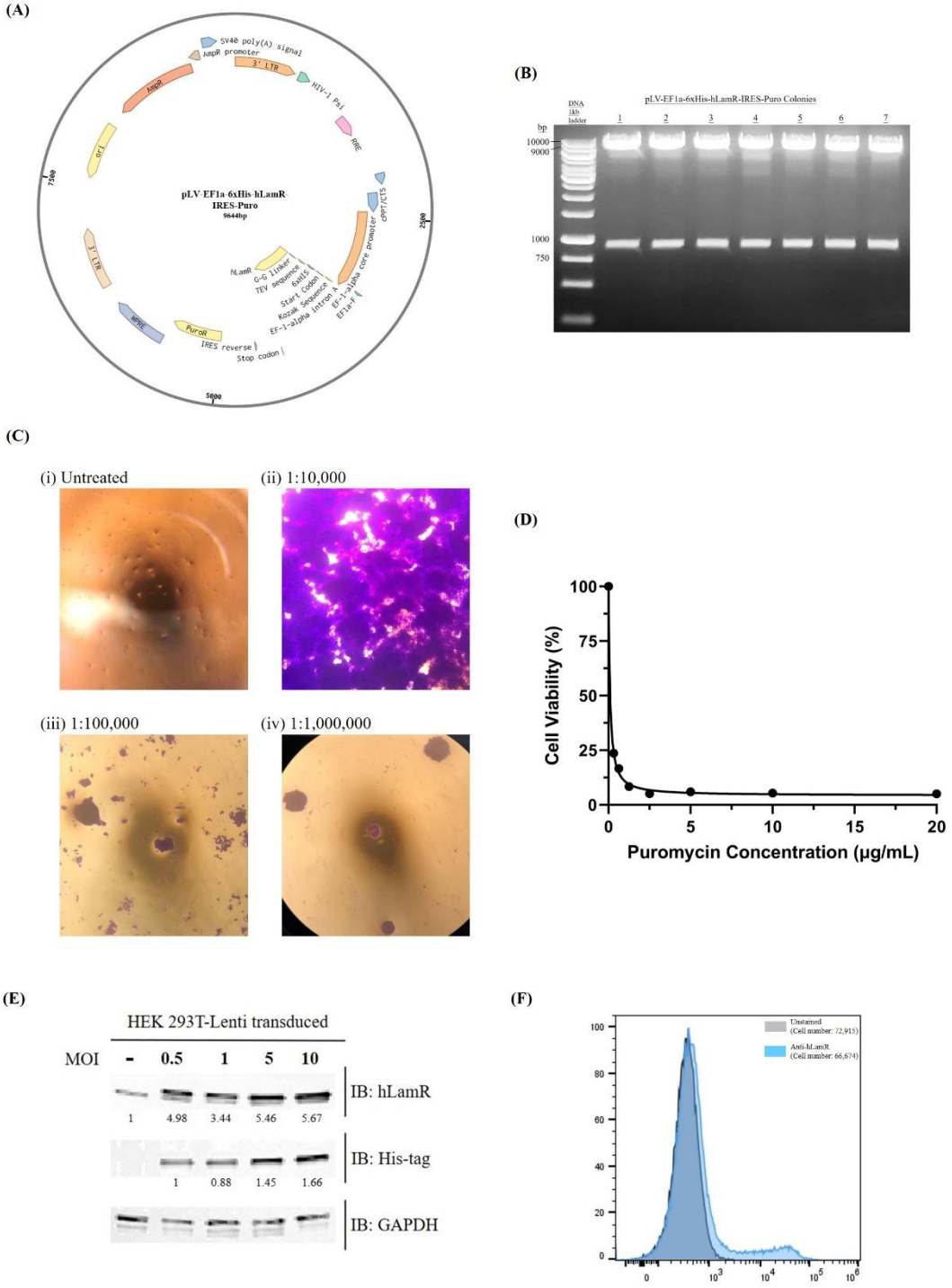

Figure 6. Stable hLamR expressing HEK293-T Making. (A) Map of pLV-EF1a-6xHIS-hLamR-IRES-Puro. **(B)** The constructed lentiviral transfer plasmid was confirmed by co-digestion of BamHI and EcoRI. The desired insert size is 942bp. **(C)** Naïve HEK-293T cells were infected by serial diluted hLamR-lentivirus, and then on the third day, started to treated with 2.5 μg puromycin as the selection agent, the cells were incubated continually within puromycin containing medium for 6 days. $1{:}10^{-4}$ virus dilution showed a lawn which was not countable, whereas $1{:}10^{-5}$ and $1{:}10^{-6}$ have 402 and 55 colonies. **(D)** Naïve HEK-293T cells were treated with different concentrations of puromycin, the lowest concentration (2.5μg) which could inhibit all the cell growth was selected as the concentration use for producing the stable cell line. **(E)** Western blotting validated the expression of recombinant his-tagged hLamR and the higher the MOI, the higher the expression level. **(F)** HEK293T-Lenti transduced cells (MOI 10) were labelled with anti-hLamR antibody to understand the surface expression level of hLamR.

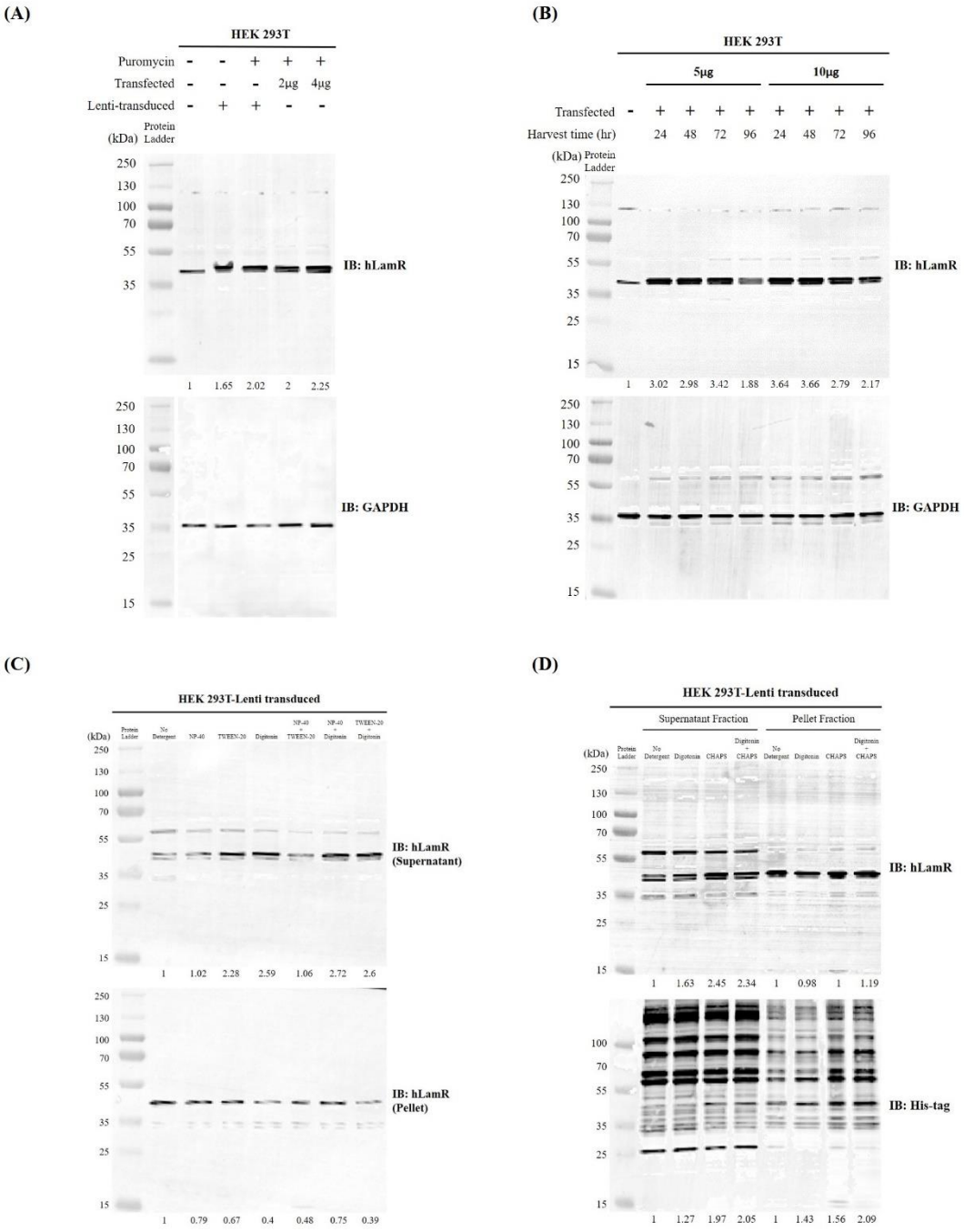

Figure 7. Optimization on Recombinant hLamR Expression and Protein Extraction. (A) Evaluating the expression level in stable lenti-transduced cells, with and without puromycin in the culture medium, and transient transfected cells. The membranes were incubated with anti-hLamR antibody and anti-GAPDH antibody, respectively. **(B)** Optimizing recombinant hLamR expression through transfecting different amounts (5 or 10μg) of pLV-EF1a-6xHIS-hLamR-IRES-Puro plasmid and harvesting cell at mutiple timepoints post transfection. The membranes were incubated with anti-hLamR antibody and anti-GAPDH antibody, respectively. **(C)(D)** Optimizing protein extraction by adding surfactant and combination of surfactants into lysis buffer. Both the fractions of supernatant and pellet from cell lysates were harvested. The membranes were incubated with anti-hLamR antibody and anti-his-tag antibody, respectively. All the Relative expression levels were shown in the figures.

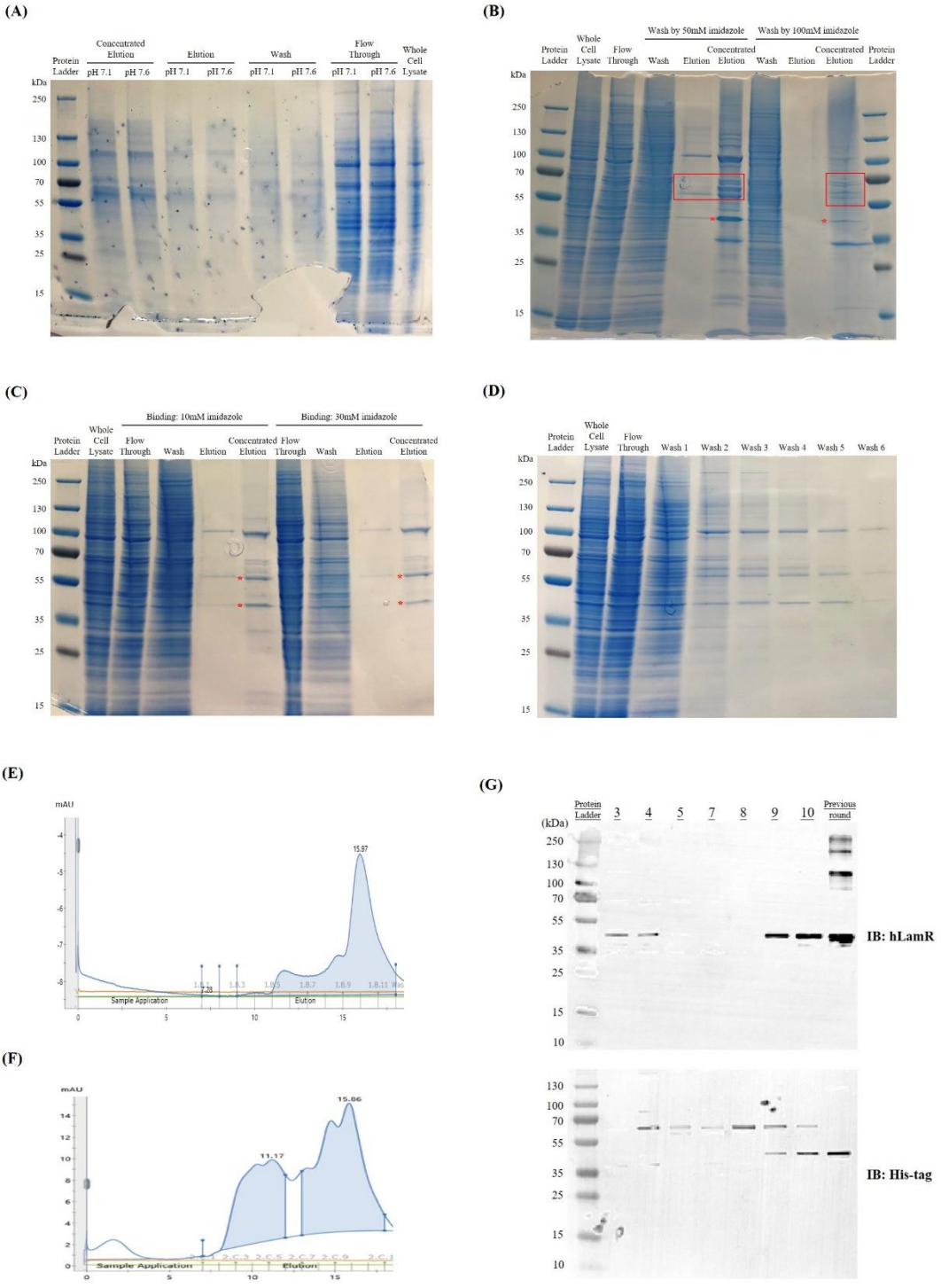

Figure 8. Eukaryotic Recombinant His-tagged hLamR Purification via Ni-NTA Affinity Chromatography. (A) 10mM, 25mM and 250mM imidazole was included in the binding, washing and elution buffer, respectively. pH 7.1 of all the buffers and pH 7.6 of all the buffers were used. **(B)** All buffers are pH 7.6. 10mM imidazole for binding, 50 or 100mM washing (5 rounds, first two are with tween-20), 300mM imidazole for elution. **(C)** All buffers are pH 7.6. 10 or 30mM imidazole for binding, 50mM for washing (6 rounds, first three are with tween-20), 300mM for elution. **(D)** Coomassie blue staining for washing time optimization. All buffers are pH 7.6. 30mM imidazole for binding, 50mM for washing (6 rounds, first three are with tween-20), 300mM for elution. **(E)(F)** Two separate rounds of size exclusion chromatography (SEC). **(G)** Western blotting confirmed the fractions out of SEC have recombinant his-tagged hLamR. The membranes were incubated with anti-hLamR antibody and anti-his-tag antibody, respectively.

Supplementary Information

(A)

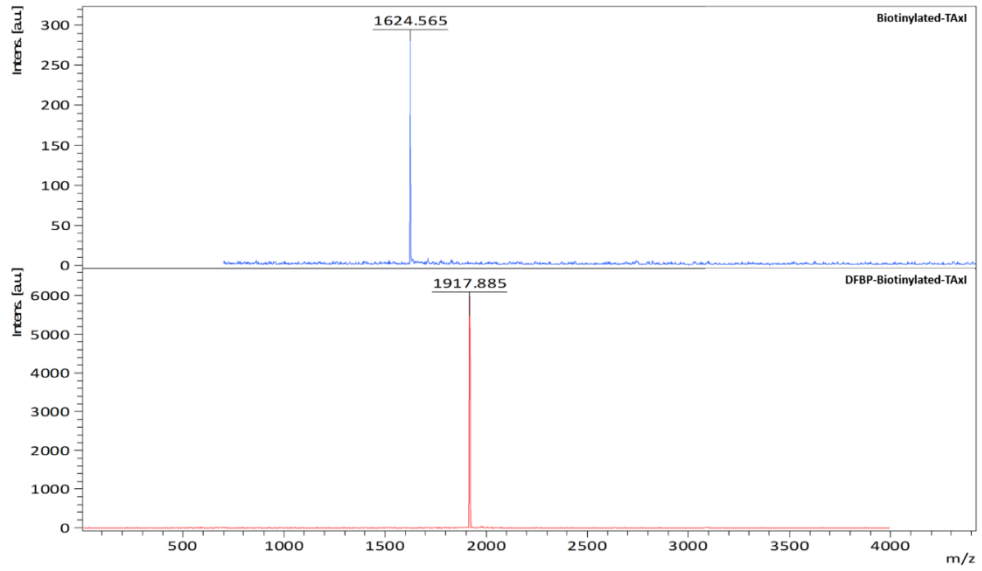

(B)